Cape Peninsula
University of Technology

Controller & modification of a Light Hub-Motor propelled Electric Wheelchair

by

Marc Alistair Matthews

Thesis submitted in fulfilment of the requirements for the degree

Magister Technologiae: Discipline Electrical Engineering

in the Faculty of Electrical Engineering

at the Cape Peninsula University of Technology

Supervisor: Dr Ian De Vries

Cape Town
18th July 2012

DECLARATION

I declare that this thesis is my work. It has not been submitted before for any degree at this institution or any other institution. All literature used has been fully referenced using the Harvard referencing system.

I hereby submit this thesis in partial fulfilment of the requirements for the Magister Technologiae in Electrical Engineering at the Cape Peninsula University of Technology.

Submitted by: 

Marc Matthews

On the 24th October 2011

SYNOPSIS

Due to the complex design of existing electric mobility vehicles in South Africa and their imported parts, make them unaffordable to the majority of disabled people in South Africa. The traditional electric units are also not practical for use in rural areas due to the heavy, bulky design. The scope of this study was to investigate various designs using existing wheelchair frame designs, low cost three phase hub motors and various electronic techniques to achieve the desired functionality. An attempt was be made to remove inefficient and expensive DC brush motors and the gear boxes associated with the traditional design of wheelchairs, while still allowing the unit to fold like the traditional manual chair design.

One of the aims for this electric wheelchair was to utilise existing large radius wheels, typical of manual wheelchairs and a modified traditional frame design, providing the clearance often necessary to overcome rough terrain whilst enabling the chair to be used as a manual wheelchair should the battery fail. One of the primary aims of the project was to develop a method for an electric assist feature built into the modified electric wheelchair, whereby the force applied to the manual pushrims on the wheels would be measured and the electric component would proportionally assist the user. This option suits the users who are weak but not physically disabled. One of the many focal points here would be on HIV/AIDS patients, which is prevalent in South Africa, who may require a wheelchair when debilitated with this disease. The electric assist portion of the design would act similarly to a wireless self-powered torque sensor, allowing for an array of applications besides the electric assist portion of this project.

A recent survey by National Government indicated that over 85% of wheelchair users only generated an income of between R0 – R500 per month. Low state disability grants and wage figures for disabled and HIV/AIDS patients mean that electric mobility vehicles have become a luxury rather than an essential commodity in South Africa. The need for cheap electric wheelchairs that could cope with the rural terrain and could be fitted onto existing manual wheelchairs offering the full manual operation should the batteries go flat, was clearly apparent. The cost of an electric wheelchair ranges from R18 000 with more advanced models escalating in price to well over R150 000. These prices were typically the result of the complexity of the unit and local wheelchair manufacturers having to import 80% of their parts from abroad. The largest local manufacturer is CE Mobility which is the dominant

mobility vehicle supplier in Southern Africa and has the only SABS approved units for sale. Our complete redesigned wheelchair including the manual frame supplied by an existing supplier would only cost R9 000. A prototype demonstrated that is was possible to build a wheelchair that meets all these criteria. A cost effective unit could provide a solution to assist and enable economically challenged and disabled people in rural areas of Southern Africa.

ACKNOWLEDGEMENTS

I would like to thank the following people and organisations that have supported me through various stages in this project.

Thanks to:

- Dr Ian de Vries as my supervisor for his invaluable advice.
- All the staff and students in the CIR who guided me through the project.
- South African National Energy Research Institution (SANERI) for funding the project through a two year bursary.
- The national Research Foundation (NRF) for making funding available for all the laboratory equipment purchased.

TABLE OF CONTENTS

DECLARATION i
SYNOPSIS ii
ACKNOWLEDGEMENTS iv
LIST OF TABLES ix
LIST OF FIGURES x
GLOSSARY OF TERMS xiv

CHAPTER 1 ..... **1**
Introduction 1
Background 1
Joystick operation 1
Electric assist operation 2
Problem statement 2
Project objectives 3
Delineation of the project 3
Thesis outline 3

CHAPTER 2 ..... **5**
Literature Review 5
Wheelchair modification introduction 5
Brushless hub motor propulsion 5
BLDC motor wheelchair modification 5
Electric wheelchair control considerations introduction 7
Joystick control techniques 7
Wheelchair control techniques 9
Wheelchair electric assist technique introduction and study 13
Literature review conclusion 24

CHAPTER 3 ..... **25**
Wheelchair Modification 25
Wheelchair modification design introduction 25
Manual wheelchair composition and design motivation 25
Manual wheelchair frame redesign 26

Overview of the three-phase hub motor and required propulsion forces 28
Final wheelchair hub assembly 30
Wheelchair modification conclusion 31

CHAPTER 4 ..... **33**
Wheelchair electric assist 33
Wheelchair electric assist introduction 33
Electric assist design block diagram and design considerations 33
Force measurement 34
Strain gauge sensors 34
Pushrim design 35
Force measurement using strain gauges (attempt 1) 36
Force measurement using strain gauges (attempt 2) 37
AD620 Instrumentation amplifier 40
Measurement electronics power stage 42
Wheelchair electric assist conclusion 44

CHAPTER 5 ..... **45**
Joystick design and construction 45
Static joystick design introduction 45
Joystick design considerations 45
Joystick design conclusion 49

CHAPTER 6 ..... **50**
Wireless power generation 50
Wireless power generation introduction 50
Power source considerations 51
Radio Frequency power transfer option 51
Battery operated power source option 52
Slip Ring power transfer option 53
Transformer coupling and current transfer 53
Mechanical design with considerations 55
Primary and Secondary coil design 56
Initial encased coil design considerations 57
Final encased coil considerations 59

Combined Primary and Secondary coil resonant frequency measurement and calculations 63
Primary coil square wave generator 64
Primary coil square wave oscillator final circuit and description 65
Secondary coil, rectification and smoothing circuit considerations 66
Wireless power generation conclusion 67

CHAPTER 7 ..... **69**
Wireless measurement electronic transfer 69
Measurement electronics with wireless signal transfer introduction 69
Wireless signal transfer considerations 71
RF signal transfer method considerations 71
Tuned circuit wireless power transfer consideration 72
Signal transfer using a parallel resonant circuit 72
Balanced slope detector considerations 73
Frequency-in versus voltage considerations 74
Signal transfer coils combined calculations and considerations (first stage of experimentation) 74
Initial stage 75
Primary feed 76
Secondary receiving 76
Conclusions to the initial test 77
Wireless signal transfer design summary 78
Final wireless signal transfer electronic design considerations 80
Wireless measurement electronics results and conclusions 84
VCOin(primary) versus Vout(secondary) 84

CHAPTER 8 ..... **85**
Overall conclusions and results 85
Project overview 85
Wheelchair redesign conclusion 85
Electric assist option conclusion 85
Static joystick design conclusion 86
Wireless power generation conclusion 87
Wireless measurement electronic signal transfer conclusion 88

Project obstacles and limitations 88
BIBLIOGRAPHY **90**
APPENDIX A ..... **i**
APPENDIX B ..... **iii**
APPENDIX C ..... **v**
APPENDIX D ..... **vi**
APPENDIX E ..... **vii**

LIST OF TABLES

Table 1: Control word table programmed into the Voice Master Key……11

Table 2: Final Voltage in VS Voltage out results 84

LIST OF FIGURES

Figure 1: Block diagram detailing the Korean design 6

Figure 2: Block diagram depicting the Integral System for Assisted Mobility 12

Figure 4: Dielectric disks displaying their electromagnetic properties while in resonance 19

Figure 5: Capacitively-loaded loops displaying their electromagnetic properties at a distance D 19

Figure 6: Analytical expressions showing optimum resonant frequency estimations for r = 6cm and r = 12cm 21

Figure 7: Prototype block diagram of the design 22

Figure 8: Prototype block diagram 23

Figure 9: Typical manual wheelchair 25

Figure 10: Solid Edge (CAD) wheelchair hub motor fixing design 27

Figure 11: Final machined hub fixed to the wheelchair frame 27

Figure 12: Forces acting on the wheelchair showing the necessary holding force required at a 12° incline 28

Figure 13: Internal structure of the 400 series hub motor 29

Figure 14: Complete left wheelchair assembly 30

Figure 15: Full mechanical redesign showing the complete left and right wheel configurations 31

Figure 16: Basic block diagram illustrating the design stages 34

Figure 17: Strain gauge shown as the serpentine structure and showing the directions of sensitivity 35

Figure 18: Traditional wheelchair pushrim configuration with the 180 degree fixing iron visible 36

Figure 19: The top view of the first design, the identical configuration was used for the underside of the flat iron bar 36

Figure 20: Two strain gauges and two dummy resistors in the Wheatstone bridge configuration 37

Figure 21: Redesigned pushrim fasteners fixed at 90 degrees to the pushrim, allowing for a greater bending moment 38

Figure 22: Solid Edge redesign of the pushrim strut showeing the 90 degree bending line 38

Figure 23: Strain gauge pair A and Strain gauge pair B configured at 180 degrees apart on the opposite sided struts 39

Figure 24: The full Wheatstone bridge configuration including the four strain gauges, allowing for a maximum potential difference when force was applied to the pushrim by the user 40

Figure 25: Measurement system block diagram 41

Figure 26: The second stage of the measurement designed circuitry 42

Figure 27: Measurement electronics PC board 43

Figure 28: Spring steel bend at 90 degrees with two strain gauges mounted on each side 45

Figure 29: Prototype joystick assemblies constructed out of spring steel while mounted on aluminium angel iron 46

Figure 30: Two strain gauges and two dummy resistors in the wheatstone bridge configuration 46

Figure 31: Joystick operational block diagram 47

Figure 32: Two different views of prototype joystick housing made out of PVC plastic 48

Figure 33: Wheatstone bridge with current regulating and voltage capping/current regulating resistors, extracted from the measurement electronic circuit.....50

Figure 34: Actual size of a typical 6V 0.5Ah SLA battery.....52

Figure 35: Typical transformer model 54

Figure 36: Typical transformer model with an airgap 55

Figure 37: Illustration of the redesigned wheelchair frame, showing the rotating barrier where the wireless power transfer was required.....55

Figure 38: The primary and secondary mounting positions 56

Figure 39: Illustrates the machined inner nylon core, aluminium mould, top and bottom view of the first prototype polymer and iron filing cast 57

Figure 40: Initial nylon coil with 60 turns cast in the iron filing and polymer mixture 58

Figure 41: A-Illustrating the purchased E shaped transformer laminations, B-illustrating the final prototype U shape lamination after modification.....59

Figure 42: The first stage of the coil prototype manufature. A nylon inner winding hub was machined to support the 0.5mm diameter coated copper tranformer winding wire. The copper wire was wound to 15 turns using a cordless drill 59

Figure 43: The second stage of the coil prototype manufacture. Standard transformer laminations were manually measured and cut to size using a pair of tin snips 60

Figure 44: Third stage, the cut tranformer laminations and inner coil winding assembly. The laminations were modified to best fit the inner transformer core.....60

Figure 45: Final stages of assembly. The laminations were placed as tightly on the inner core as possible. The final lamination count was 250 61

Figure 46: The casting process of the inner copper core with laminations, before a pure polymner was poured into the mould.....62

Figure 47: Depicts the final prototype. The primary and secondary transformer generator coils are shown mounted onto the fixed wheelchair frame and moving hub and wheel assembly. The final fixed distance from primary to secondary coils was 1mm 62

Figure 48: The inverter (MOSFET) square wave oscillator operational diagram 65

Figure 49: Final MOSFET square wave oscillator circuit 66

Figure 50: Rectification, regulation and referencing stage electronics 67

Figure 51: Digital illustration of the primary and secondary coils at 1mm apart 68

Figure 52: Final prototype strain gauge setup for the user force measurement 69

Figure 53: Typical Wheatstone bridge configuration 70

Figure 54: Typical balanced slope detector operation 73

Figure 55: Illustration detailing the first stage of the design using the 250mm diameter 1mm thick wire, glued onto the perspex sheet maintaining the 1mm airgap 75

Figure 56: Typical initial primary feed circuitry 76

Figure 57: Typical initial secondary circuitry 76

Figure 58: Initial manual frequency sweep test results 77

Figure 59: Mechanical redesigned power and signal transfer coil pair with a signal coil turns ratio of 1:1 79

Figure 60: Mechanical redesigned power and signal transfer coil pair with a signal coil turns ratio of 1:2 80

Figure 61: Typical secondary rectification and voltage doubler circuitry 81

Figure 62: Graph detailing the results found with the signal transfer coils wound smaller at a turns ratio of 1:2 with the voltage doubler on the secondary 82

Figure 63: Graph indicating the input and output load variations 83

Figure 64: Final prototype graph indicating the final results 84

GLOSSARY OF TERMS

DC – Direct Current

PM BLDC – Permanent Magnet Brushless Direct Current

MVFH – Minimum Vector Field Histogram

CIR – Control Instrumentation Research department

CPUT – Cape Peninsula University of Technology

PC – Personal Computer

PCB – Printed Circuit Board

CMOS – Complementary metal–oxide–semiconductor

N – Newton

IC – Integrated Circuit

PID – Proportional, Integral and Derivative

FPGA – Field Programmable Gate Array

PSUBOT – Portland State University roBOT

POT – Potentiometer

MUX – Multiplexer

VI – Virtual Instrument

ERSG – Electrical Resistance Strain Gauge

FNTM – Field Node Transceiver Module

PSK – Phase Shift Keying

BSTM – Base Station transceiver Module

VNA – Vector Network Analyser

WCP – Wireless Charging Pad

PWM – Pulse Width Modulation

IR – Infrared

VCO – Voltage Controlled Oscillator

SLA – Sealed Lead Acid

CHAPTER ONE
Introduction

1.1 Background

A survey by National Government (Propenta (PTY) Ltd, 1999) indicated the cost of an electric wheelchair started at R18,000.00 with more advanced models escalating in price to well over R150 000 (Medop cc, 2006). These prices are typically a result of local wheelchair manufacturers having to import 80% of the electric wheelchair parts from overseas for local assembly. With low state disability grants and low wage figures for disabled workers, electric wheelchairs have become a luxury rather than an essential commodity in South Africa. Furthermore, existing motorised wheelchairs based on first world designs do not cater, and are insufficiently robust for the African terrain and climate.

The study shows that the traditional wheelchair design could be modified to accommodate a low cost motor design, driven by state-of-the-art power electronics with a retail price of below R 10 000.00. The scope of this study was to investigate low cost, three phase hub motors in an attempt to remove inefficient and expensive DC brush motors and the worm drive gear boxes, associated with traditional electric wheelchair designs. The goal was to utilise existing large radius wheels, typical of manual wheelchairs, providing the clearance often necessary to overcome rough terrains of Southern Africa, whilst enabling the chair to be used as a manual wheelchair should the battery fail. To achieve this, high torque, 3 phase hub motors were chosen for the design, with advanced three phase inverter topology. The primary focus of the study was to design an electric assist option whereby an input by the user results in mechanical force assistance, proportional to the users input. A second control technique studied was a uniquely designed joystick, controlling each wheel individually.

1.2 Joystick operation

This stage of the design used two static joysticks to control each of the wheels individually. The joysticks were bi – directional using advanced measurement instrumentation electronics, to measure the force applied by the user. The force

applied was proportional to the electrical energy, converted into kinetic energy by the (BLDC) Brushless Direct Current hub motors. The static joystick design was maintenance free due to frictionless movement of the components, opposed to multiple moving parts as in the traditional joystick design.

1.3 Electric assist operation

The electric assist option allowed the user to manually maneuver the wheelchair, by using both hands pushing on the metal pushrims, while fixed to the outside of the large radius wheels. While propelling the unit, the force applied by the user was measured and transmitted wirelessly to the frame of the wheelchair. The proportional force applied by the user was converted into kinetic energy, by the state-of-the-art power electronics and BLDC hub motors fixed to the wheelchair.

1.4 Problem statement

The complex design and imported parts of existing, locally manufactured electric wheelchairs make them unaffordable to the majority of disabled people in South Africa. The traditionally designed electric wheelchairs are not practical for use in rural areas due to the heavy, bulky design. If the batteries go flat there is no way of moving the unit without a recharge. Many wheelchairs are used purely for mobility assistance by users who maybe weak due to a debilitating disease. These types of users may only require an electric wheelchair on odd occasions when they are too weak to maneuver the units themselves.

The purpose of this study was to examine the redesign of a standard wheelchair into a motorised vehicle accommodating the people living in rural and urban areas, while handling the South African terrain. The investigation covers a control technique aimed at persons that were weak but not fully disabled, like users that would require some mechanical assistance while self-propelling themselves on the wheelchair. Furthermore, wheelchair users want to feel and be independent, an electric assist option allows persons to be more independent due to the mechanical assistance. The study included researching traditional wheelchair frame modification, and readily available hub-motors, previously utilised in an electrical bicycle project by the CPUT

CIR, and developing control techniques utilising strain measurement, to develop the final electrically assisted manual/electric wheelchair prototype.

1.5 Project objectives

The scope of this study was to investigate low cost, three phase, hub motors in an attempt to remove inefficient and expensive DC brush motors and the gear boxes associated with traditionally designed electric wheelchairs. The goal was to utilise existing large radius wheels, typical of manual wheelchairs, providing the clearance often necessary to overcome rough terrain whilst enabling the chair to be used as a manual wheelchair should the battery fail. To achieve this, high torque, three phase hub motors were chosen and associated three phase inverter topologies developed. Research will be done on two controller types, namely a static type joystick per wheel and a wireless force control system fixed on the independent pushrims on the wheels of the wheelchair. The two types of control techniques were designed to accommodate the weak users, debilitated by disease. The overall scope of the project was to ensure a cost effective solution aimed at poor South Africans living in the rural areas of the country.

1.6 Delineation of the project

The research will include the redesign of a traditional manual wheelchair into an electric propulsion type using cost effective hub motors and power electronics. Two control techniques will be investigated allowing for controlled outputs proportional to the users mechanical inputs. The hub motor driver utilising the control signals fell out of the scope of this thesis.

1.7 Thesis outline

In Chapter 1 the thesis topic is introduced detailing the problem statement influencing the project scope.

In Chapter 2 the literature review is detailed relating to the dissertation.

Chapter 3 details the wheelchair frame upgrade design.

Chapter 4 outlines the electric assist research with the user force measurement.

Chapter 5 details the unique joystick design and development.

Chapter 6 discusses the wireless power generation on the independently rotating wheelchair wheel for the measurement electronics.

Chapter 7 details the technique adopted for the wireless signal transfer from the wheel to the frame of the wheelchair.

Chapter 8 concludes all the design phases of this project.

The Bibliography and Appendices follow.

CHAPTER TWO
Literature Review

2.1 Wheelchair modification introduction

The study highlighted the need for cost effective electric wheelchairs. Many disabled or disease weakened users own state issued manual wheelchairs which influenced the re-design of an existing manual wheelchair to accommodate an electric propulsion system, directly modifying these wheelchairs into an electric unit. Further studies indicated the need for advances in the motorised control of these modified electric wheelchairs, which will be discussed further in this paper.

2.2 Brushless hub motor propulsion

The research led to the utilisation of 3 phase brushless DC Hub motors for the wheelchairs modification due to their compact design and high power output. Recent research indicates that the current drive systems for light mobility vehicles and electric wheelchairs consists of brushed permanent magnet DC motor and mechanical transmission on the wheels. The overall efficiency of this kind of drive usually did not exceed 60%. (Chikkam, 2005). Presently under study were more effective drive systems consisting of brushless DC motors, which were embedded into the wheel rim while directly driving the wheelchair wheels. These types of high efficiency gearless drives were the objectives of the first stage of this study. The particular brushless DC motor was a torus – type motor with high energy rare – earth magnets and ferromagnetic teeth that fill the space between the coils.

2.3 BLDC motor wheelchair modification

The apparent demand for electric wheelchairs globally influenced researchers in Korea to design and build an electric wheelchair using BLDC hub motors mounted onto a conventional manual wheelchair utilising large radius wheels (Chu, Moon, Choi, Ryu, Mun 2004).

The control architecture of the design consisted of two layers of feedback control, namely the wheelchair posture control and the wheel velocity control. The Posture controller operated as a reference velocity generator for the wheels, this was at the higher level of the control architecture. The lower level architecture comprised of the velocity controller performing in four quadrant operations. A block diagram of the design follows below.

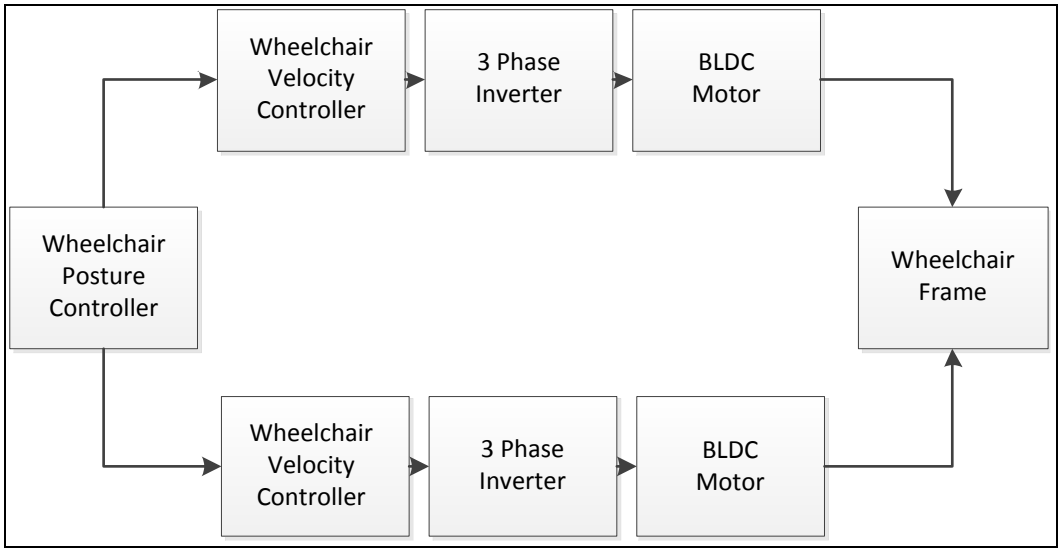

Figure 1: Block diagram detailing the Korean design

The Korean design technique influenced the mechanical design of the wheelchair discussed in this thesis. A similar design strategy was adopted utilising BLDC hub motors with large radius wheels, directly fixed onto a manual wheelchair frame. However the Korean researcher's primary focus was on the BLDC motor three phase motor driver, the posture and velocity controller. The BLDC motor controller used in this paper's design was designed and built by Dr Ian De Vries of the CIR at the CPUT. It was utilised on an electric bicycle using a similar three phase inverter design as the Korean researchers.

The performance, design and low cost of these Brushless DC Hub motors ensured that the optimum propulsion design specification was met for this project. The goal of the project was to utilise existing large radius wheels, typical of manual wheelchairs and modify the original frame to accommodate the fixing of the Brushless DC Hub Motors, providing the clearance often necessary to overcome rough rural terrain whilst enabling the chair to be used as a manual wheelchair should the battery fail. A

power source for wheelchair battery charging may not be readily available in the rural areas of South Africa, making this type of electric wheelchair design practical.

2.4 Electric wheelchair Control consideration introduction

While researching, designing and constructing the new electric wheelchair the need for specific motor control became apparent. A few options were considered with two standing out. A static type joystick and an electric assist type controller option controlled by a sensor that sensed the manual force applied by a rider to the hand rim. There proved to be little literature available that mimicked the proposed joystick and electric assist options researched, but various control techniques were researched before the decision was taken to continue with the designs.

2.5 Joystick control techniques

Conventional joysticks used on electric wheelchairs incorporated four quadrant control which proved difficult to operate by disabled users with severe neuro-muscular disorders like cerebral palsy and Parkinson's disease. These type of debilitating diseases result in user tremors, poor coordination and low strength, making the conventional type of joystick control unreliable and erratic.

2.5.1 A study in the United States (Myers, Wobbrock 2005) investigated the use of PalmOS devices using stylus keyboard control and EdgeWrite text entry as control techniques on an electric wheelchair. Many disabled persons used computers regularly so adapting a PC type Palm unit for control made sense. The stylus keyboard entry wheelchair control was conducive to persons with less sever neuro-muscular diseases like muscular dystrophy while the new EdgeWrite text entry technique for users suffering from severe motor neuron diseases like multiple sclerosis. The study also aimed at users who fatigued rapidly ensuring that the control mechanism used minimal effort. The EdgeWrite technique was considered as the paper detailed the use with a wheelchair joystick.

EdgeWrite is a unistroke type input technique that relies on physical edges and corners to provide stability during motion. The user moves a finger, stylus or joystick

alone the physical edges and into the corners of a square bounding the input area of the touch screen. The input recognition does not rely on the entire path of motion, but on the order corners are hit. This means that slight uncontrolled input tremors do not deter accurate recognition.

The adaption of an existing manual wheelchair joystick was considered for this thesis but this highlighted the high cost of existing electric wheelchair components. Utilising existing electric wheelchair components digressed from the scope as the design needed to be cost effective.

2.5.2 A study by the University of Freiburg in Germany developed a four degree of freedom solid state joystick using a rigid polymer cylinder with a spherical dome on top of a CMOS chip. The sensor IC contained ten octagonal stress sensors mounted across the surface using the piezoresistive effects in silicon. A linear response was shown by the joysticks stress sensors to forces of up to 5N and to a moment Mz up to 5mNm. The design mirrored the solid state joystick for the wheelchair, using fixed components and measuring strain through peizoresistive effects (Gieschke, Richter, Joos, Ruther, Paul 2008).

2.5.3 Further studies showed the design of a static joystick using a hall-effect sensor and a fixed magnet on a shaft (Lu, Kim, Lee, Li 2006). The hall sensor detected a horizontal vector in the magnetic field. The research showed the nonlinear characteristics of the output of the hall-sensors and the movement of the joystick bar. The dynamic horizontal vector of the magnetic flux is detected by the hall-sensor while the permanent magnet is moved with the joystick, while using a two-dimensional detecting area. To overcome the nonlinear characteristics of the movement vs. the output of the hall-sensors, nonlinear compensation equations were used to assist in linearising the output signal and give higher accuracy in two-dimensional movement. The work showed that the single hall-sensor design was superior to a dual sensor structure in sensing two-dimensional motion.

These studies indicated that various sensor techniques were developed to assist users in electric wheelchairs by utilising proportional force measurement of static components but not solving the issue surrounding users with neuro-muscular

disorders. The idea for the static wheelchair joystick was influenced by the measurement of static components ensuring build costs are kept to a minimum. This design technique will be discussed in detail further in this thesis.

2.6 Wheelchair control techniques

Various wheelchair control techniques were researched to assist with the design of the wheelchair user control. Different control technique research follows:

2.6.1 Literature indicated that certain individuals with disabilities lacked the co-ordination to control a joystick on a motorised wheelchair or other mobility vehicles. The avoidance of obstacles was difficult. This study aimed to implement a multi-modal system to control the electric wheelchair using a voice recognition system and sensors to detect and avoid obstacles. (Fezari, Bousbia-Salah, Bedda 2005)
The design implemented a microcontroller and voice recognition electronics for isolated words from a microphone mounted on the unit. This allowed the user to control the wheelchair using vocal control.

2.6.2 **S**tudies showed the development of a voice-controlled wheelchair for the handicapped by Portland University (Stanton, Sherman, Rohwedder, Fleskes, Gray, Minh, Espinoza, Mayui, Ishaque, Perkowski 1990: 669-672) using an on-board computer. Users with certain physical limitations found it difficult or even impossible to control an electric wheelchair. Persons suffering with cerebral palsy had issues with the co-ordination required to control a traditional electric unit safely. It was also relevant that persons without control of their arms, persons who were both blind and quadriplegic are further examples of shortcomings associated with wheelchair users with awkward disabilities.

The institution developed a computerised, voice controlled wheelchair called PSUBOT (Portland State University roBOT). The first version of the project used a standard electric wheelchair as the base with the following subsystems:

- Voice recognition control

In version one of the project a voice operated wheelchair controlled by an 8086 based personal computer was designed. The control voice was moved to a parsing algorithm whose output was used to independently control each wheel.

The joystick was simulated using a digital to analogue converter and the design control program. The aim was overall stability and to allow the computer to hold a desired speed and direction despite any possible change in angle or slope. Full manual operation of the wheelchair was available in the event of any system failure. Optical sensors were incorporated into the wheel design to sense the distance travelled by the wheels.

The wheelchair was fitted with a joystick that controlled two opposing 10kΩ potentiometers. Each wheel was controlled by an individual POT. A reference voltage of 6.8Vdc was supplied to the POT's wiper. The two opposite sides of both the POTs were coupled to two opposing pairs of differential amplifiers, one pair being NPN, while the other being PNP. The centre portion of the wiper was the neutral point for the circuit. The voltage range of the design fell between 6.8VDC and 2.3VDC with the centre position holding at 3.2VDC, while a supply voltage of 3.2VDC was fed to the pair.

- Feedback

Two direction sensing encoders were connected to the wheels, providing feedback in relation to the wheels' rotation. The encoder outputs were fed into an 8-bit counter. Interrupts could be generated at selectable intervals (of displacement) by choosing (via a MUX) which output bit of the counter generates the interrupt request to the computer. For straight line travel or a gentle turn, every 128 pulses were monitored, but for a sensitive maneuver, it was needed to sense every 64, 32 or 16 pulses.

- Voice Input System

The concern with the PSUBOT was the response time and recognition reliability of the electronics. This was provided by a Voice Master Key, a complete hardware/software package constructed to interface to an IBM PL/XT/AT/386 and

compatibles. The various control words were programmed into the Voice Master Key package and for the first version of the project was sufficient. The control words can be seen in table 1 below.

Table 1: Control word table programmed into the Voice Master Key

Zero	One	Two	Three	Four	Five
Six	Seven	Eight	Nine	Turn	Right
Left	Back	Forward	Stop	Go	Goto
Voice	On	Off	Rotate	Slow	Fast
Feet	Inch	Power	Arc	Ahead	StopStop

Vocal control as a wheelchair control technique was considered amongst many other control methods for this wheelchair project, but decided against due to cost and specific scope requirements. Different control technique research was necessary to ensure a broad understanding of all wheelchair control methods, defining the final design utilised in this dissertation.

2.6.3 At the University of Alcala in Spain research was done on command generation by face movements applied to the guidance of electric wheelchairs for handicapped people. (Bergasa, Mazo, Gardel, Barea, Boquete 2000: 660 - 663 vol.4)

A 2-D colour face tracking and fuzzy detector system was used to generate commands to drive the wheels on the wheelchair. The system was non-intrusive allowing freedom of head movements and visibility. The electronics were able to learn the face movements of the user automatically during setup. Below follows a block diagram of the system explaining the various layers associated with the project.

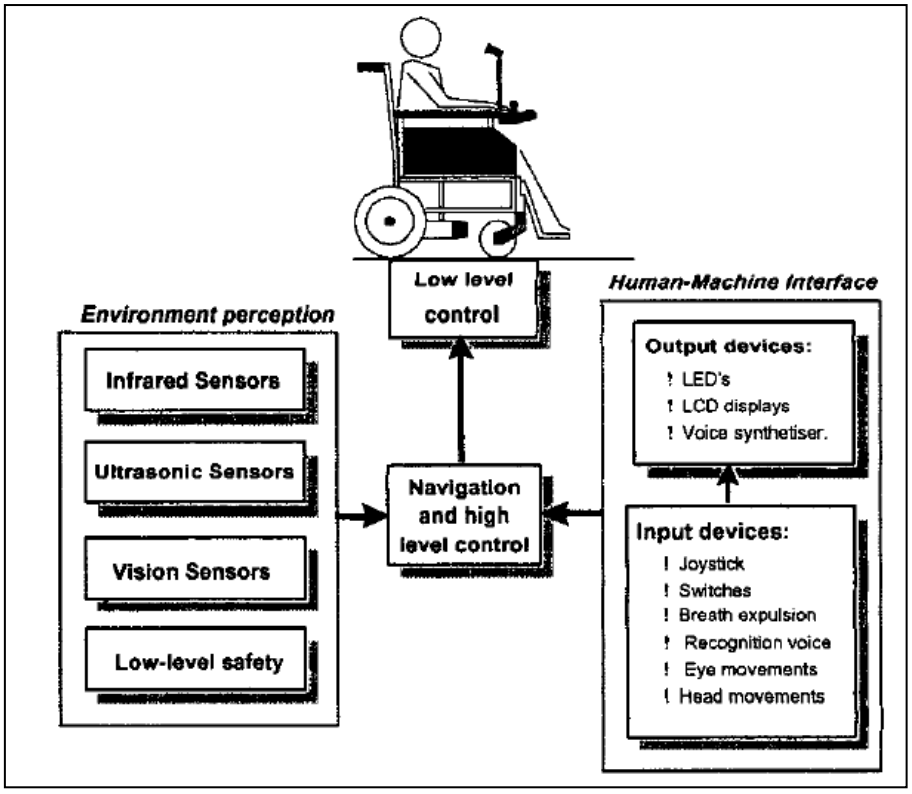

Figure 2: Block diagram depicting the Integral System for Assisted Mobility

2.6.4 With the increase in the aging society and the increase in handicapped persons, the need for improved mobility assist within their living conditions was required. Operating a motorised wheelchair indoors in confined spaces required a lot of skill. (Kurozumi, Yamamoto 2005) This research presented an obstacle avoiding support system for electric wheelchairs. The avoidance system used a semi-automatic Minimum Vector Field Histogram (MVFH) method. The MVFH changes the individual's manipulation and assists to avoid obstacles. The modification rate was changed by reinforced learning according to the user condition and environment.

2.6.5 Further studies presented the implementation, design and testing of an adaptable, optimal controller for motorized wheelchairs. Pattern recognition techniques and optimal control theory were combined to produce the design of a Variable Structure Controller (VSC) using a modified Proportional, Integral and Derivative (PID) control method. (Brown, Inigo, Johnson 1990). The controllers appropriate set of control coefficients may have been automatically selected depending on the load parameter estimates to allow a self-adaptive controller, or selected manually before installation

depending on the user's specific needs. The manually-adaptable controller was implemented on a microprocessor topology.

2.6.6 Recent research on motor controllers indicate that they required various functions, not only real time control but also communication capabilities with remote host computers and other motor controllers for synchronization. (Choi, Seo, Kim 2004). The study presents a BLDC motor controller for tele-operation by incorporating RTLinux and FPGA technologies. The designed controller was composed of an embedded RTLinux board with a StrongARM microcontroller made by Intel co. Ltd., capable of an Ethernet connection, a fast current controller implemented by using a FPGA, and a two channel BLDC motor driver for precision current control.

The previous literature showed that various types of control methods have been developed and tested. All the different designs from head movement control, face movement control and speech and sensor control were focused on users with specific disabilities. The research done in this dissertation focuses on users who are physically weak and not disabled for the electric assisted control and the joystick control for users who suffer from neuro-muscular diseases.

2.7 Wheelchair electric assist technique introduction and study

The design of an electric assist option allowed the user to manually maneuver the wheelchair, by using both hands pushing on the metal pushrims, fixed to the outside of the large radius wheels. While propelling the unit, the force applied by the user was measured and transmitted wirelessly to the frame of the wheelchair. The proportional force applied by the user was converted into motor assist torque, by the state-of-the-art power electronics and BLDC hub motors fixed to the wheelchair.

The design comprised of two components, namely the force (torque) measurement on the independently spinning wheels and a form of wireless power transfer to power the measurement electronics on the independently spinning wheelchair wheels. The following literature describes techniques for wireless torque measurement.

2.7.1 A study in Brazil (Filho, Belo, dos Santos, dos Anjos 2010) presented the design and development of a dynamic torque meter applied to rotating shafts using strain gauges, electronic transduction, telemetry and LabView programming. The measurement signal was transmitted by digital modulation from a base station unit fixed directly onto the rotating shaft to a PC, by means of VI (Virtual Instrument) developed in LabView. Conventional coupling techniques were disregarded as the use of digital modulation to transmit the measurement radio frequency signal allowed for communication with a high signal/noise ratio. The dynamic remote measurement unit used super batteries as a power source allowing for continues use for several days, with long periods between maintenance. The goal of this design was to design and build torque transducers that fulfill a broad ranges of action, high definition, low depreciation over time, that are easy to install and have low manufacturing costs.

Currently there are many highly accurate devices for measuring torque that are used for obtaining static torque only. Industry had great interest in the development of dynamic torque measurement units that display characteristics similar to those of highly accurate static devises. Presently popular torque meters use resistive strain gauges to obtain torque in rotating shafts. The ERSG (electrical resistance strain gauge) display characteristics such as calibration stability, minor variations caused by environmental factors, accuracy, dynamic response compatible with frequencies over 100 kHz allowing for remote operation, with excellent response to temperature changes, low cost, widespread use, ease of installation and operation and a linear response in a range of applications.

Dynamic torque meters primary focus is allowing data transfer with minimal noise caused by shaft rotation while ensuring a high resolution and an extended working life. These meters commonly utilise the slip ring method for power and data transfer. They consist of a set of guide rings coupled to the shaft and a series of stationary brushes, which maintain constant contact with the rings, allowing for information and power transfer. Slip ring technology displays unwanted characteristics of wear and tear through abrasion. Noise is caused by friction between the brushes and rings in applications running above 10 000rpm, care must be taken to avoid problems caused by heating and vibration.

A method using rotating transformers was developed to avoid issues caused by slip ring technology. The elimination of brushes and rings resulted in less long term wear and tear and reduced parasite torques resulting from friction. In this design the primary and secondary coils of the transformer required bearings and the coil construction was fragile. The system was also susceptible to noise and errors due to the misalignment of the two coils. A specialised signal filter was required to produce a reliable signal, making the system more expensive than the slip ring technique.

Further an infrared method used for data transmission used a rotating transformer to supply the power for the strain gauge bridge torque measurement unit. An Analogue to Digital converter in the shaft transmitted its output signal via infrared light from the rotating shaft to the stationary receiver wirelessly. This method resulted in similar abrasive wear and tear of the power brushes and rings but displayed high signal to noise ratios due to the digital transmission of data. The conclusion was that this method proved to be more costly than the previously discussed methods.

Other techniques investigated were obtaining the torque measurement by reading the torsion angle of the shaft. The shaft needed to display good resolution and have a high frequency of resonance. This resulted in the need for robust encoding to achieve high sensitivity for measurement of small torsion angles as the maximum torsion angle for the sensitive part was in the range of 0.25o per meter of shaft length.

Recent studies were done on torque measurement using fiber Bragg grating sensors replacing the ERSG and magnetostrictive sensors that change shape according to the magnetic field to which it was applied. These both resulted in complex designs and implementation with restricted applications.

This study focused on using radio frequency instrumentation for signal transfer from the independently spinning shaft to the stationary base station. The strain gauges fixed onto the shaft detected the shaft deformation, while the signal was processed and amplified by the electronic transduction circuit and sent to the FNTM (field node transceiver module). A microcontroller converted the analogue signal into digital and transmitted it to a transceiver module. The transceiver modulated the signal in phase (phase shift keying – PSK) and excited a full duplex antenna, transmitting the signal

via radio frequency. The Transceiver module in the base station BSTM (base station transceiver module) received the signal via a helical antenna then filtered and demodulated it making it available for reading. The signal output was available in the standard 4 to 20mA pattern and/or the MODBUS industry standard protocol. The schematic of the design follows the diagram below.

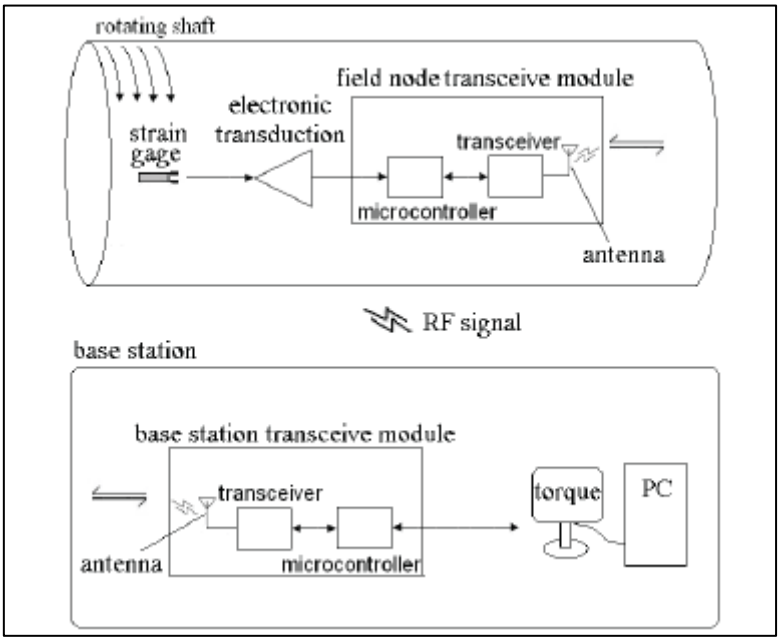

Figure 3: Schematic of the design proposed by this study

2.7.2 A similar study in Portugal (dos Santos, dos Anjos 2011) presented a self-powered torque meter, using strain gauges, telemetry and LabView for the design and implementation of the project. An electronic transduction signal was also transmitted by digital modulation from a remote transduction unit fixed on the rotating shaft to a base station sending signals using virtual instrument in LabView. The wireless protocol used in this experiment utilised ZigBee/IEEE 802.15.4 protocol for communications, which is highly used in industrial monitoring and control applications.

Various dynamic torque sensing techniques were described that could have been utilised in the design for wireless force measurement, applied by the user on the pushrims. The technique for torque/force measurement and transfer will be discussed in the upcoming chapters indicating the influence the studied literature had on the

final design. The following studies describe various wireless power transfer techniques.

2.7.3 A study on invasive medical devices like mico-robots (Li, Yan Gao 2010) for gastrointestinal inspections, video endoscopic capsules, and telemetric capsules for physiological parameter monitoring showed that they were primarily powered by cell batteries or via cabling when operating in the human body. The clinical applications of these devices were confined due to the power limitations. The resolution to this was to adopt a method of transcutaneous energy transmission to power an artificial heart resulting in high efficiencies due to the fixed position and orientation of the power-transmitting and power-receiving coils.

This article focused on a method of wireless power transmission based on electromagnetic localisation and synthesis ensuring sufficient power was supplied to the endoscopic capsule without increasing the electromagnetic field strength to levels that might harm humans. By nature the power-receiving coil in the capsule changed position and orientation randomly affecting the efficiency of the power transmission. Conventional methods determined that to maintain the operating power in the capsule, the source power needed to be increased to unacceptable levels. The focus was to use this proposed method but ensuring the power transfer efficiency remained high, avoiding the increase in energising currents.

The experiments performed in this study showed that the system of wireless power transmission could automatically tune the power-transmitting coils, to a sufficient resonant state, while regulating the power needed by the capsule. The efficiency of the system remained high when ensuring the compound vector of the energising magnetic field remained orthogonal to the cross-section of the power-receiving coil. The localisation experiments proved that the position error was 10mm with the orientation error being 2°, satisfying the need for calculating the orientation of the synthesised vector.

However, some defects to the design were found. The localisation system experienced interference when operated near electromagnetic devices, because of the eddy current effect by large metal bodies. The efficiency of the wireless power transmission was affected due to the non-uniformity of the synthesised electromagnetic field, by which the power could be transmitted wirelessly.

The power transfer method adopted in this literature of electromagnetic coupling, enabling wireless power transfer while displaying transformer type characteristics was noted and considered as the most likely way to generate the necessary wireless power. Further wireless power transfer techniques are described further.

2.7.4 A study at MIT (Massachusetts Institute of Technology) in the USA (Karalis, Joannopoulos, Slojačić 2008) investigated whether efficient energy transfer over non-negligible distances could be achieved by utilising the phenomenon of long-lifetime resonant electromagnetic states with localised slowly-evanescent field patterns. An analysis for efficient medium-range wireless energy transfer was performed through detailed theoretical and numerical techniques of real-world models and realistic parameters. Efficient coupling was achieved in this study.

The proposed method used was based on the popular principle of resonant coupling (similar-frequency resonant objects tend to couple) and resonant evanescent coupling (coupling mechanism is mediated through the overlap of non-radiative near-fields of two objects). These types of resonant coupling allows for efficient wireless power transfer at close distances to one another. This literature investigated the efficient wireless power transfer for distances larger than the largest dimension of both objects involved in the transfer (Medium distance). Research was done on two different, but well-known electromagnetic resonant systems, namely 2D dielectric disks and capacitively-loaded conducting-wire loops. Both mediums displayed acceptably good performance. The study focused on mathematical models describing the characteristics of the materials while in resonance with one another to achieve power transfer. The orientation of the dialectic disks and the capacitively-loaded

conducting-wire loops were of interest for the wheelchair power transfer model in this dissertation, disregarding the need for the complex mathematical models described in this study. Below in figure 4 and 5 the orientation of both mediums is shown. The image below serves to illustrate how the researchers utilised visual modelling to conclude their experiments, the relevance to the wheelchair project only focuses on the coupling aspects of this project at a fixed distance.

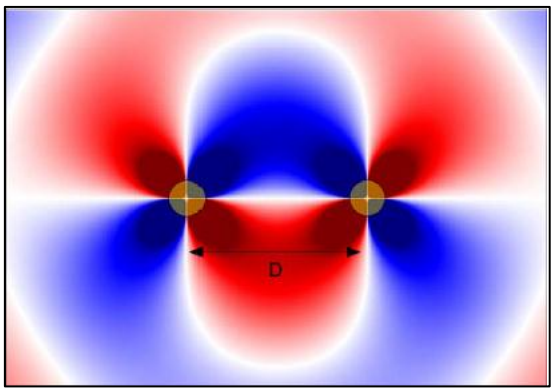

Figure 4: Dielectric disks displaying their electromagnetic properties while in resonance D

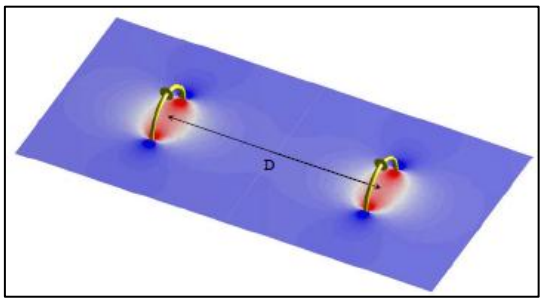

Figure 5: Capacitively-loaded loops displaying their electromagnetic properties at a distance D

The literature studied highlighted the efficiency and higher power outputs gained by utilising the conventional method of inductance coupling at a resonant frequency. The following studies focuses on this type of wireless power transfer.

2.7.5 This study in Canada (Kaminska, Mahanfar, Mazlouman 2009) focused on the optimisation of energy transfer of inductive coils using magnetic resonance at mid-range distances of around 10 – 100cm. These types of coils could have been used for powering wireless sensors and battery-operated devices. The similar phenomenon of optimal energy transfer at resonance of a system was identified. Numerous

prototypes were developed, validating the designs while displaying an efficiency of around 25%, when the optimum resonant frequency was achieved with accurately matching circuitry.

Optimised inductive linked circuits have displayed efficiencies of up to 90% for short distances within 1 – 3cm. However, the efficiencies of such inductive links significantly dropped for longer ranges at a decay rate of 1/r3. The efficiencies throughout the distance ranges improved as the systems were forced to tune to a resonant frequency, with far higher efficiencies experienced at very close ranges. In addition to the pair of coils distance dependant efficiencies, the coil specifications such as core material, number of turns, size, load variations and coil alignment were parameters influencing the function of the optimum resonant frequencies. By measuring the network parameters an estimate of the optimum frequency and energy transfer efficiency was found.

The proposed method adopted several prototypes like two pairs of medium size coaxially aligned coil pairs of radius 6cm and 12 cm verifying the performance of the system. This paper described efficiencies of about 25% with the coil pair fixed at a size of 12cm at a distance of 10cm, the efficiency dropped to 4% when the distance was increased to 0.5m. Similarly, the coils displayed efficiencies of 16.5% at the fixed size of 6cm at a distance of 10cm, the efficiency dropped to 2.5% at a distance of 0.5m.

Firstly the design was theoretically modeled using the standard quality factor and resonant frequency calculations defined as:

$$Q = \frac{\omega.L}{(R_{ohm} + R_{rad})} \text{ (equation 1)}$$

and

$$\omega = \frac{1}{\sqrt{LC}} \text{ (equation 2)}$$

Respectively, where L being the inductance of the coil, C the parallel equivalent capacitance of the coil (inclusive of self-capacitance and parasitics) and R_{ohm} and R_{rad} being the wire inside loss and radiation resistance (radiated energy),

respectively. The impedance of the wire coil with N turns, a radius r of conducting wire and a circular cross section of radius a, surrounded by air, can be described in the following equation as:

$$L = \mu_0 N^2 r \left[\ln\left(\frac{8r}{a}\right) - 2\right] \text{(equation 3)}$$

Figure 6 below shows a plot of Q versus frequency and highlights the optimum frequency of energy transfer of two sets of coils with parameters: (a) the r = 6cm coil pair with N = 12 turns and wire cross section radius of a = 0.36mm and (b) the radius r = 12cm coil pair with N = 6 turns and wire cross section radius of a = 1.2mm.

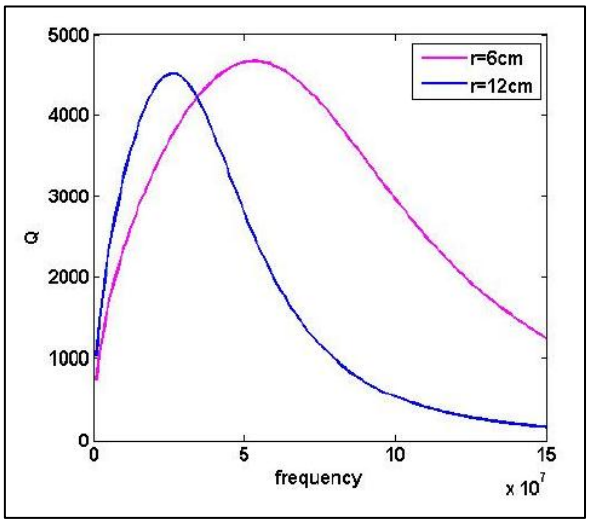

Figure 6: Analytical expressions showing optimum resonant frequency estimations for r = 6cm and r = 12cm

The optimal energy transfer frequency (maximum Q) was estimated at around 54MHz for the smaller r = 6cm coil pair and around 27MHz for the larger r = 12cm coil pair. Things to note was that the predicted theoretical values for f, Q or efficiency were not accurate due to reasons like the smaller set of coils resonating at higher frequencies. The analytical equations were based on low frequency modelling and do not consider the influence of parameters to the frequency. Many assumptions were made that could substantially affect the higher frequency performance estimations.

The study further focused on utilising a vector network analyser (VNA) to characterise the resonant frequency, as well as the self and mutual impedance of the coil pair. This was achieved by representing the system as a two-port network.

The detailed analytical models described further in this study had minimal relevance to the wheelchair wireless power transfer. The tuned resonant circuitry utilising two coils at a fixed size and distance apart were relevant and influenced the wheelchairs wireless power transfer design. The final block diagram of this prototype is shown in figure 7 below.

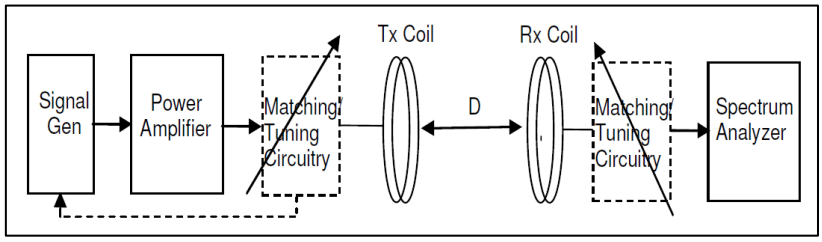

Figure 7: Prototype block diagram of the design

In conclusion the prototypes constant resonant frequency was set to 30.55MHz giving an efficiency of 25% for the 12cm coil, and 16.5% for the 6cm coil at a measured distance of 10cm. The efficiency dropped to 4% for the 12cm coil and 2.5% for the 6cm coil pair at a distance of 50cm. Theoretical modelling of the resonant systems provided some useful data but system parameters influence the outputs dramatically. The external influences of the parameters described in this study highlighted the necessity for prototype designs, for the wheelchairs wireless power and signal transfer using magnetic inductance coupling at resonance.

2.7.6 Research in Hong Kong (Leung, Chan, Lit, Tam, Chow, 2010) designed and built a wireless power transmission system consisting of a wireless charging pad (WCP) as the transmitter and a charging receiver unit. The charging receiver was a multi-function device that plugged directly into electronic devices such as mobile phones and PDA's, providing the device with necessary charging power. The idea with this design was to replace conventional wired chargers with a wireless system avoiding direct contact charging hazards. The transmitting unit (pad) consisted of a power source and a coil, where the receiving unit consisted of a similar coil whereby magnetic induction was achieved. Figure 8 below shows a block diagram of the prototype.

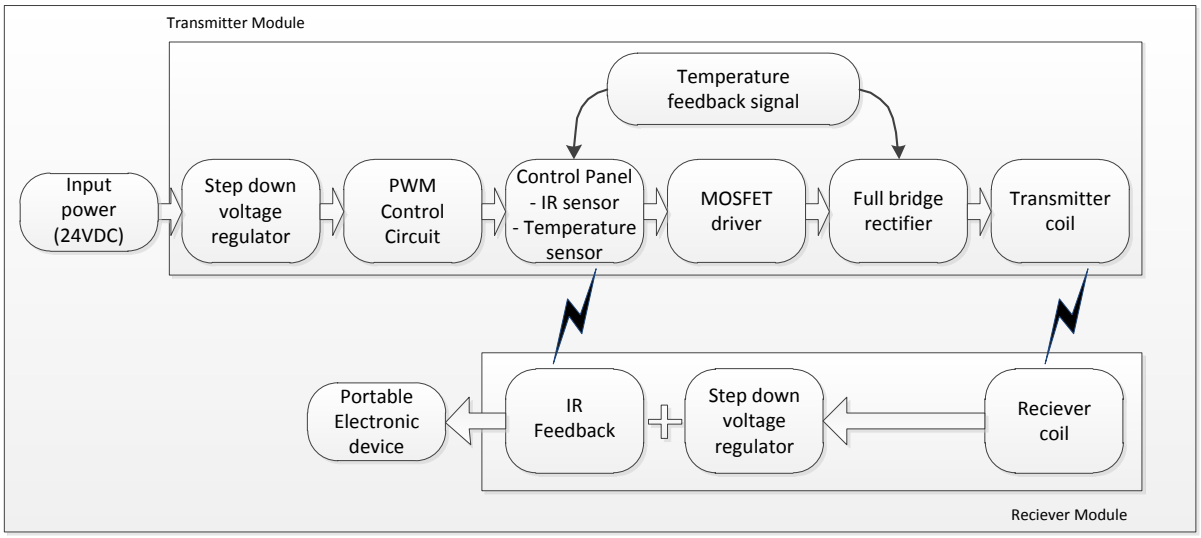

Figure 8: Prototype block diagram

The input voltage was set to 24VDC which is lower than the safe voltage standard limitation of 36VDC. The voltage regulator in the first stage of the circuit provided the necessary circuit buffering, voltage maintenance and minimising the noise from the source for the high frequency circuit. The Pulse Width Modulation (PWM) control circuit utilised a basic PWM IC to simply generate a highly fluctuated square wave in order to produce the magnetic field at the transmitter coil. The control panel of the design composed of two sections to monitor the state on the WCP, one was the overheating prevention system and the other the load detection Infrared Sensor. The MOSFET driver was controlled by a standard 555 timer and on detection of a load via the Infrared (IR) sensors the MOSFET driver would compare the control signal and the 555 timer signal setting an oscillation in process. The output signal of the MOSFET driver controlled a full bridge rectifier converting the DC signal to an alternating square wave. Full-wave rectification generated a high power changing voltage suitable for magnetic field generation in the transmitting coil.

A thick multi-core induction coil was utilised for the transmitter coil to reduce heat loss and skin effect due to the high frequency signals. The manufactured coil could withstand much higher voltages and currents and ensured better efficiencies. The primary and secondary coils of the transmitter and receiver comprised of 10-12 turns at a distance of 10cm.

On the receiver a voltage rectifier was used to change the alternating current/voltage to a usable DC voltage. Furthermore a 5VDC voltage regulator was used to steady the usable DC voltage for use by the IR load detection circuitry and finally the output.

2.8 Literature review conclusion

The referenced studies discussed above were all carefully considered while developing and designing the wheelchair prototype in this dissertation. The literature reviewed may seem vast, but a greater understanding of a broad spectrum of wheelchair control techniques and designs needed to be considered to ensure the final prototype design followed the necessary engineering trends.

CHAPTER THREE
Wheelchair Modification

3.1 Wheelchair modification design introduction

The study highlighted the need for cost effective electric wheelchairs. Many disabled or disease weakened users own state issued manual wheelchairs. This influenced the re-design of an existing manual wheelchair to accommodate an electric propulsion system allowing for direct modification of the disable or weak user's wheelchair into an electric unit. This chapter describes the technique used to modify an existing manual wheelchair to accommodate the fitment of electric hub motors with large radius wheels suitable for South Africa's rural terrains. A prototype was constructed and detailed in this chapter.

3.2 Manual wheelchair composition and design motivation

A standard manual wheelchair comprises of the following basic components:

A. Wheels with plastic rims
B. Small front guide wheels
C. Footrests
D. Frame containing fabric seat and backrest

Figure 9: Typical manual wheelchair

The basic design of a standard issue and locally manufactured manual wheelchair is shown in figure 9 above. Various techniques were considered for the electric wheelchair design with one being apparent. Modifying a standard manual wheelchair seemed to be the practical solution as the majority of existing wheelchair users in South Africa already own one. By simply modifying an existing manual wheelchair allowed for the opportunity to upgrade a user's existing manual wheelchair, saving the cost of an entirely new manual wheelchair. This type of wheelchairs primary market were users that earned salaries below the breadline, so cutting unnecessary costs was a primary objective.

3.3 Manual wheelchair frame redesign

A study at the Cape Peninsula University of Technology by Dr Ian De Vries designed and built an electric bicycle comprising of a 3-phase DC brushless hub motor mounted onto the front forks of the bicycle with advanced control electronics. The electric hub motor for the bicycle was available over the counter from china. This specific bicycle influenced the modification technique utilised in the motorised wheelchair design. The idea was to fix the hub motor onto the manual wheelchair frame and fix a large radius type wheelchair rim and tubeless tire onto the hub motor via standard specification bicycle spokes.

A CAD (Computer Aided Design) program called Solid Edge was utilised to design the various mechanical components of the wheelchair. A mounting hub was required to fasten the hub motors fixed shaft onto the wheelchair frame. Through experimentation a number of designs were considered, the final fixing hub prototype CAD design is shown in figure 10 below. All measurements for the machining were referenced off the existing wheelchair frame diameter and the hub motors fixed shaft radius. The wall thickness of the hub was overdesigned ensuring adequate strength.

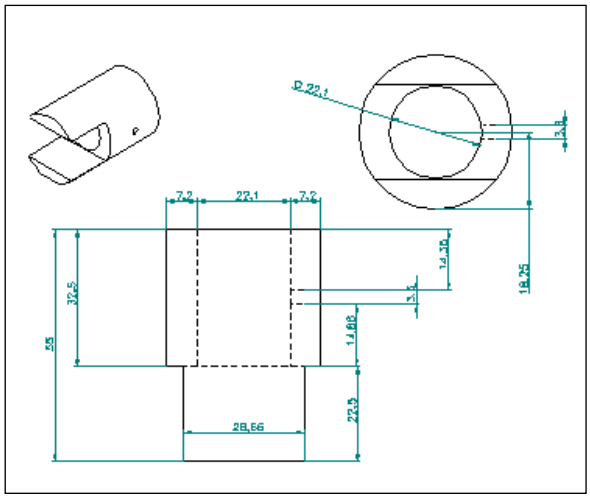

Figure 10: Solid Edge (CAD) wheelchair hub motor fixing design

Due to the budget constraints of this project a structural engineer could not be employed to do a final inspection of the hub and fixing technique adopted. A simple matter of user experiments was used to ascertain whether the machined hub would hold the appropriate weight. The trail tests determined that a user of an average weight of 100kg could comfortably be held by the designed hub and motor assembly. Future studies on a second revision would require a structural engineer's hub design with exact loading calculations recorded and documented. The prototype machined hub welded to the existing wheelchair frame is displayed in figure 11 below.

Figure 11: Final machined hub fixed to the wheelchair frame

The metal hub shown in figure 11 above was machined out of a solid hi-tensile steel rod. The existing plastic wheels (see figure 9 above) fixing supports were cut off and the new hub fit snugly around the frame.

3.4 Overview of the three-phase hub motor and required propulsion forces

The pancake shape of these hub motors were the best choice for the direct drive of the motorised wheelchair as they could be inserted directly into the hub of the wheel and provide drive to the outer wheelchair rim and tubeless tire via the spokes. These motors also produced sufficient torque for the application, the force diagram and calculations follow below (Matthews, 2006).

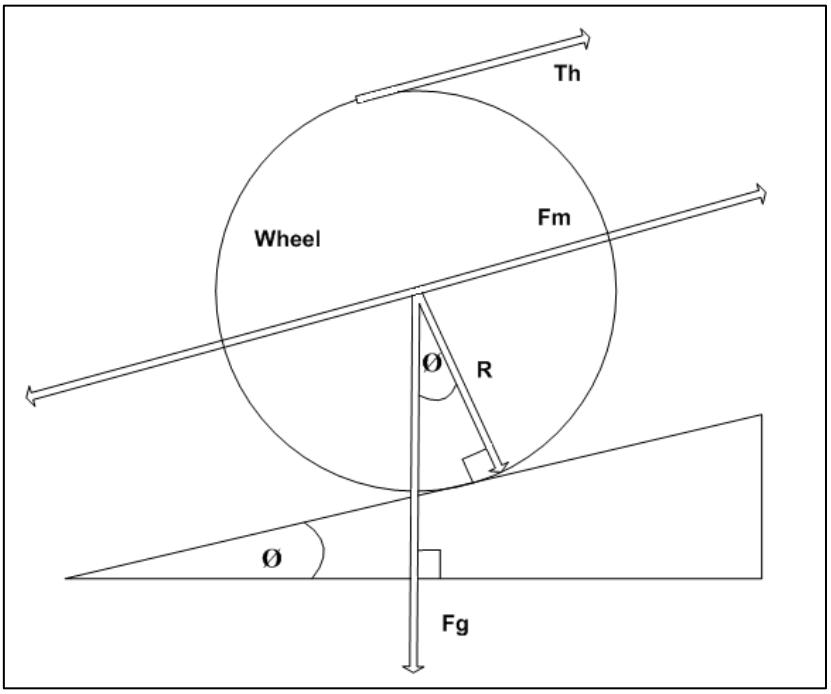

Figure 12: Forces acting on the wheelchair showing the necessary holding force required at a 12° incline

The forces acting on the wheelchair were used to calculate the amount of torque required to climb a 12º hill, an average male's weight of 80kg was used for the calculations.

Where:

$g = 9.81 m/s$ (Gravity)

$R = 30cm$ (Radius of the drive wheel)

$m = 80kg$ (Mass of an average adult male)

$\theta = 12^0$ (Angel of Incline)

$$F_g = m \,.g \qquad \text{(Equation 4)}$$

$$F_m = F_g \,.\, \text{Sin}\ \theta \qquad \text{(Equation 5)}$$

$$T_h = F_m \,.\, R \ \text{(Holding torque)} \qquad \text{(Equation 6)}$$

From equation 6 the holding torque necessary to maintain the wheelchair on a slope of 12° was 49 newton meters (N.m). The 400 series Permanent Magnet Brushless Direct Current (PM BLDC) motor was finally considered due to their maximum output torque of 40 N.m. per motor. The combination of the two motors produced sufficient driving torque (80N.m) to easily overcome a 12° hill incline.

In figure 13 the internal structure of the 400 series PM BLDC motor can be seen. There are three separate windings wound around a mild steel core.

Figure 13: Internal structure of the 400 series hub motor

The three-phase permanent magnet DC brushless motor comprised of a fixed machined shaft and stator assembly with the outer casing being the rotor. The rotor rotates inside the hub which was lined with permanent magnets. Hall Effect sensors

are mounted between the windings, relaying a message back to the logic indicating which phase needed to be excited at which specific time. The control logic switches the correct sequence of MOSFETs exciting the phases which enable rotation.

3.5 Final wheelchair hub assembly

All the components for the wheelchairs mechanical redesign were collaborated to build the final working prototype. This is shown in figure 14 below.

Figure 14: Complete left wheelchair assembly

The complete redesign was vigorously tested with a user weighing 100kg as an ordinary manual wheelchair and it was found to be mechanically sound. The complete design showing the left and right wheel designs can be seen in Figure 15 below.

Figure 15: Full Mechanical redesign showing the complete left and right wheel configurations

The redesigned wheelchair comprised of the following components:

A. Spoked wheel with self-contained BLDC hub motor and pushrims mounted on the outside.
B. BLDC hub motor fixed into the redesigned hub.
C. Traditional wheelchair frame containing fabric seat and backrest.

3.6 Wheelchair modification conclusion

Through vagarious design changes the wheelchairs mechanical design proved to be adequate. The newly designed frame with all electrical and electronic components mounted on it could accommodate a person's weight of up to 100 kilograms. The propulsion calculations proved that with an 80kg user the wheelchair could comfortably ascend an incline of 12°.

As per the South African National Building Regulations (RSA National Government, 2006) the maximum allowable ramp inclines are 1:12 where the difference in levels of the extents of the ramp exceeds 400mm and 1:10 where such the difference is more than 400mm. These regulations show a maximum angle of 5.4° at heights up to

400mm above ground level and 4.7° for all landing heights above 400mm above ground level.

Thus showing that the wheelchair could comfortably overcome all regulation wheelchair inclines throughout South Africa.

CHAPTER 4
Wheelchair electric assist

4.1 Wheelchair electric assist introduction

The wheelchair electric assist option was considered to assist wheelchair users who are weak, but not fully disabled and users who suffer from debilitating diseases who are immobile due to the illness. A large number of wheelchair users in Southern Africa rely on manual wheelchairs when weak, due to illness. These users may only use the units on odd occasions and when necessary.

The wheelchair design incorporated a system for sensing the users mechanical force applied to the manual wheelchairs pushrims and proportionally powering the wheels individual motors. The proportionally measured signal needed to be transmitted wirelessly from the individually rotating wheels to the fixed wheelchair frame to be utilised by the advanced electronics and hub motors. In conjunction with the wireless signal transfer from the wheel to the frame the electronics on the wheels required powering, highlighting the need for a wireless power transfer system from the wheelchair frame to the spinning wheels. This will be discussed further in this dissertation.

The aim of this chapter was to investigate the force measurement of the user on the individual pushrims on the individually rotating wheels.

4.2 Electric assist design block diagram and design considerations

The following block diagram shown in figure 16 below illustrates the basic design considerations used in this project. The requirement was for a force measurement system located on each wheelchair wheel measuring the force applied to the pushrims by a user. The resulting electronic signal needed to be transmitted wirelessly to the wheelchair frame while the electronics on the wheel being powered wirelessly from the static frame.

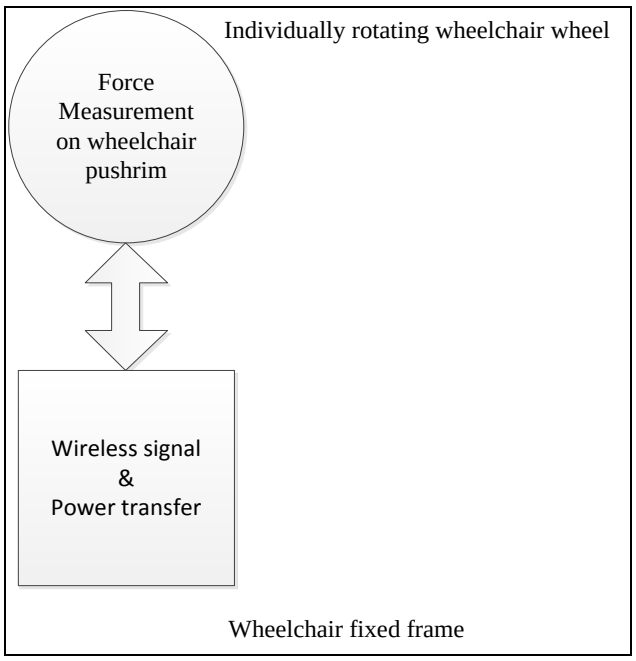

Figure 16: Basic block diagram illustrating the design stages

4.3 Force measurement

4.3.1 Strain gauge sensors

Strain gauges are resistive sensors also known as deposited resistors. The conducting resistive path in the deposited gauge is nickel or copper deposited onto a flexible material in a serpentine form. When the material is compressed in the direction of the deposited resistor or if the material is bent in a concave shape perpendicular along the axis of the resistor, then the particles are forced together making the resistance decrease - see figure 17 below. If the material is under tension in the direction of the resistor, or if the material is bent in a convex shape alone the axis, then the particles tend to separate and the resistance increases. Bending force applied along an axis parallel to the resistor, compressing, or tensional force in the direction perpendicular to the direction of the resistor does not separate or compress the particles in the gauge, so the resistance remains unchanged. These devices are highly sensitive and can be very small. The gauges are normally configured in the Wheatstone bridge configuration with all the biasing electronics. The degree of tension, bending and compression is proportional to the resistance change in the strain gauge element. (James & Carstens, 1993).

For the purpose of this study, and to ensure the costs of the research and prototype remained low the strain gauges utilised were ones readily available in the CPUT CIR store room (120Ω, 0.3% tolerance Vishay resistive strain gauges). These strain gauges had the advantage of lower costs and proving to be an established product. Thus the resistive types of strain gauge are the most commonly used in industry. Various other types of strain gauge exist namely, acoustic, capacitive, inductive, mechanical optical, piezo-resistive and semi-conductive. These were not considered for this project due to availability and cost. The primary objective of this project was to measure the strain or bending moment of the pushrim supports of the wheelchair when a force was applied by a user. The readily available Vishay strain gauges proved to be practical and cost effective for this application. With more time and a larger research budget other types of strain gauges could be researched and possibly utilised in this project. The project focus was to utilise existing materials and techniques as best possible to achieve an overall prototype proving the utilised methods of development worked sufficiently.

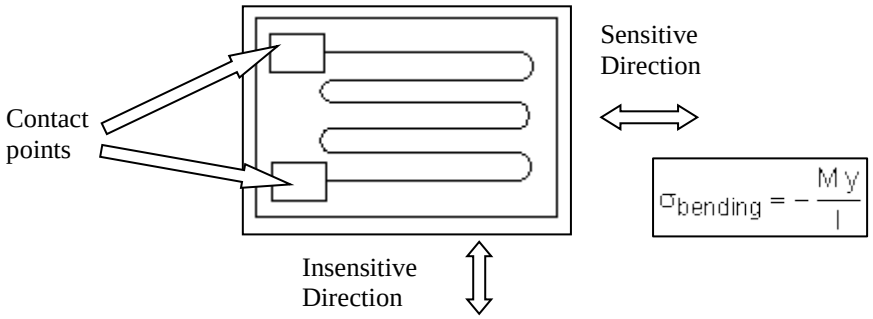

Figure 17: Strain gauge shown as the serpentine structure and showing the directions of sensitivity with the bending formula utilised to justify the strain gauge selection.

The formula above in Figure 17 was used to determine the bending stress, and is also commonly called the flexure formula. The y term is the distance from the neutral axis (up is positive). The I term is the moment of inertia about the neutral axis. The results determined the final strain gauge specifications.

4.3.2 Pushrim design

The traditional pushrim design consists of a metal ring with a diameter of 500mm fixed to the rim of the wheel with a matching inside diameter of 500mm. The pushrim was fixed to the rim by four flat iron bars connected at 90° intervals. The basic design consisted of the flat iron pieces attached to the pushrim at 180°, as shown

in figure 18 below. Figure 18 illustrates the traditional fixing points of the pushrim showing the basic flat iron connector rim configuration described earlier.

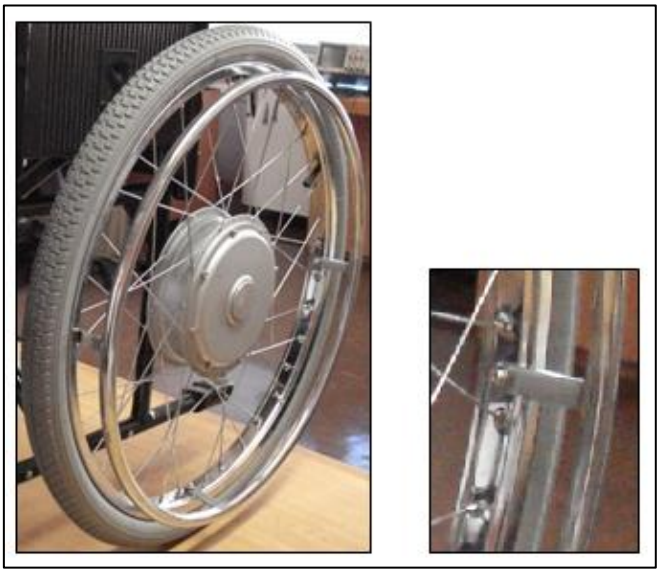

Figure 18: Traditional wheelchair pushrim configuration with the 180 degree fixing iron visible

4.3.2.1 Force measurement using strain gauges (attempt 1)

In the first attempt two 120Ω, 0.3% tolerance Vishay strain gauges were fixed onto one of the 180° flat iron bars connecting the pushrims to the wheelchair rim. The configuration is illustrated in Figure 19 below. The design was considered via considerations between the researcher and the supervisory body at the CIR (CPUT) and thus influenced the following methods of research trial and error. Without time constrains and limited budgets the method of calculating the shear bending moments of the pushrim supports could have been achieved, allowing for a possible improvement of strain gauge choice for this portion of the project.

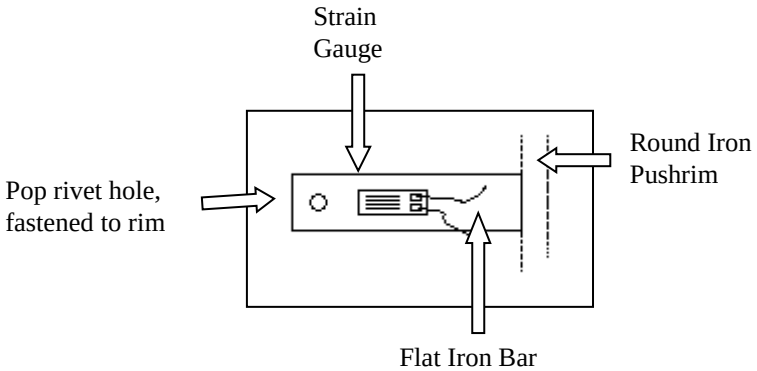

Figure 19: The top view of the first design, the identical configuration was used for the underside of the flat iron bar

The strain gauges were connected in a Wheatstone bridge configuration, with the two strain gauges forming the one half of the bridge while two dummy 120Ω resistors forming the other half of the Wheatstone bridge. The configuration of the first design is shown in figure 20 below.

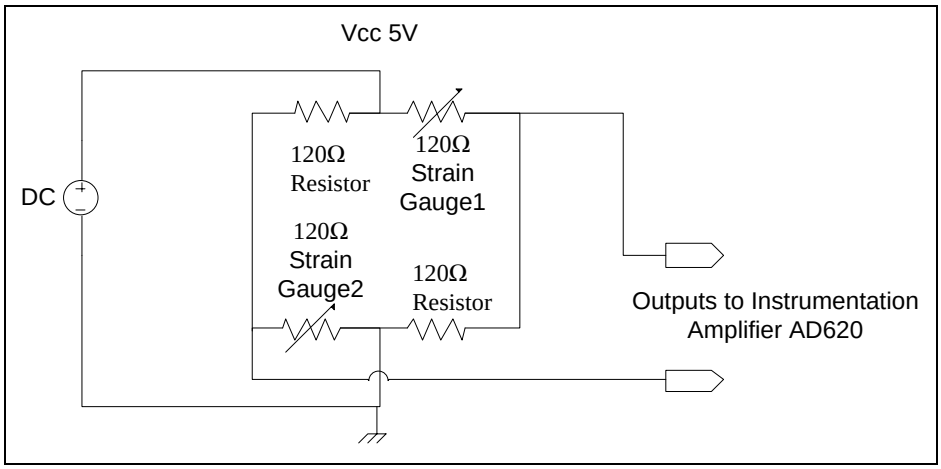

Figure 20: Two strain gauges and two dummy resistors in the Wheatstone bridge configuration

Under no-load conditions the Wheatstone bridge was balanced and the potential difference of 0V was measured at the output. Once a force was applied to the system the balance of the system changed and produced a differential output voltage proportional to the force applied.

4.3.2.2 Force Measurement using strain gauges (attempt 2)

The experiments performed in the first attempt with two strain gauges mounted and the iron flat bar configured at 180° proved that the force applied by the user was not sufficiently straining the flat bar. This design did not allow for sufficient strain on the strain gauges and enough potential difference, measured at the output of the Wheatstone bridge. A mechanical redesign of the pushrim configuration was made and implemented. This allowed for greater sensitivity of force measurement by the system by allowing a greater bending moment of the pushrim fastening flat iron bars. The mechanical redesign of the pushrims is shown in figure 21 below and described further.

Figure 21: Redesigned pushrim fasteners fixed at 90 degrees to the pushrim, allowing for a greater bending moment

The iron connecting bar was redesigned using Solid Edge v15 CAD (Computer Aided Design) program and was laser cut to ensure accuracy. A two dimensional illustration of the redesigned pushrim support bar follows below in figure 22 showing where a 90° (arrow indicated) bend was done to finalise the bracket manufacture.

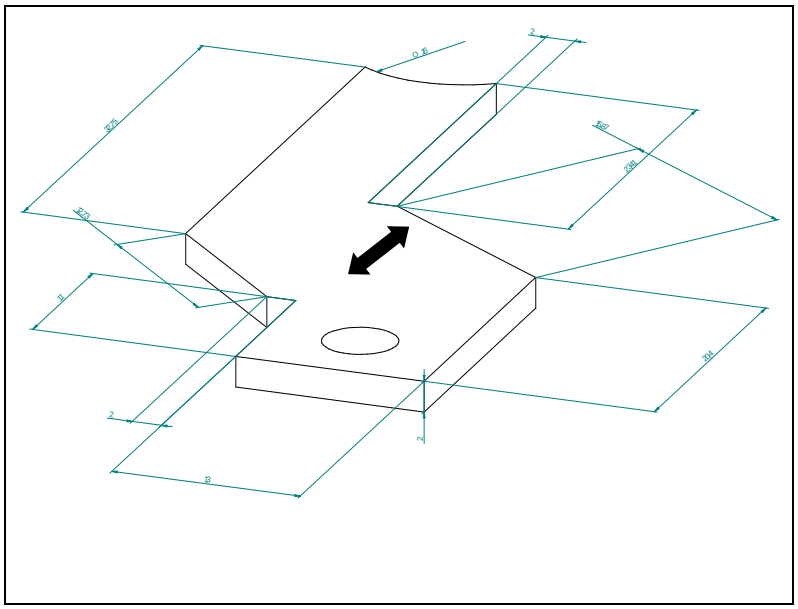

Figure 22: Solid Edge redesign of the pushrim strut showing the 90 degree bending line

In the original pushrim strut design, the flat iron bar was fixed at 180° (see Figure 18 before). The traditional configuration did not allow for enough mechanical bend (bending moment) in the iron strut when force was applied by the user, resulting in insufficient amounts of strut and strain gauge deflection. This resulted in an unusable potential difference measurement output by the Wheatstone bridge. The redesigned strut as seen in figure 21 and 22 was fixed to the pushrim at 90°. This configuration allowed for greater mechanical bend when force was applied to the pushrim and provided enough change for the strain gauges to measure.

To increase the sensitivity of the system a second pair of strain gauges were mounted to the opposite side strut (180° apart) thus eliminating the dummy 120Ω resistors and allowing for an even greater mechanical change measured by the Wheatstone bridge, finally resulting in a usable proportional potential difference output. The configuration described is shown in figure 23 below.

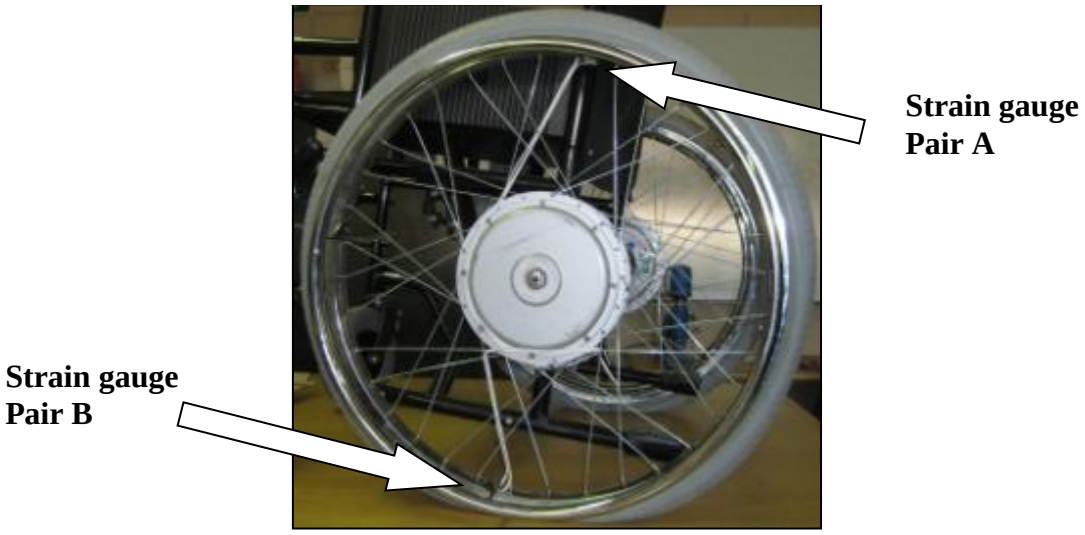

Figure 23: Strain gauge pair A and Strain gauge pair B configured at 180 degrees apart on opposite sided struts

With the addition of the second pair of strain gauges and the elimination of the dummy 120Ω resistors, the Wheatstone bridge configuration allowed for greater differential change of the balanced output when force was applied to the pushrim. This also allowed for greater potential difference voltage of the output when a proportional force was applied. The configuration Wheatstone bridge can be seen in figure 24 below.

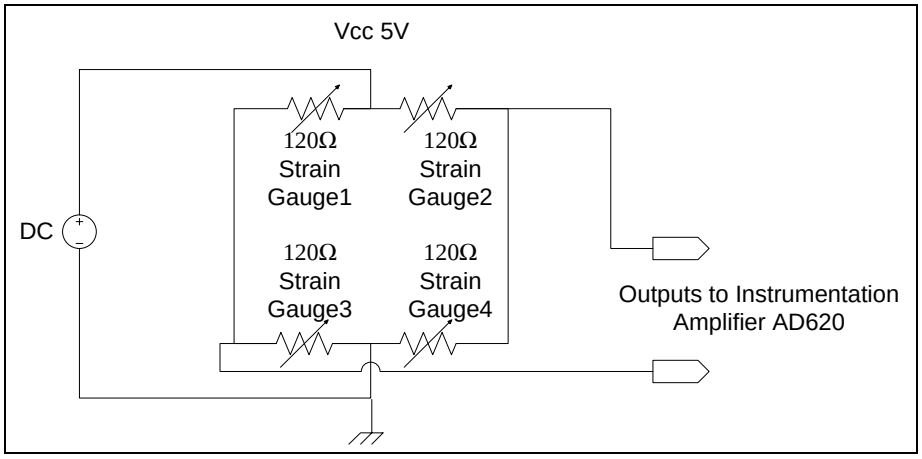

Figure 24: The full Wheatstone bridge configuration including the four strain gauges, allowing for a maximum potential difference when force was applied to the pushrim by the user

4.3.3 AD620 Instrumentation amplifier

A low cost AD620 instrumentation amplifier was used for the differential voltage measurement from the Wheatstone bridge. The low power amplifier (only 1.3mA max supply current) offered high accuracy of 40 ppm non-linearity, a low offset voltage of 50uV and offset drift of 0.6 uV/°C max (Analog Devices, AD620 datasheet, 2005). The AD620 instrumentation amplifier was capable of gains of 1 to over 1000 which proved ideal for the pushrim force measurement application. Below in figure 25 a block diagram of the measurement system can be seen. The AD620 instrumentation amplifier was chosen as it was readily available and cost effective. There are many instrumentation amplifiers available on the market, but due to cost, practicality and time implications the AD620 was utilised.

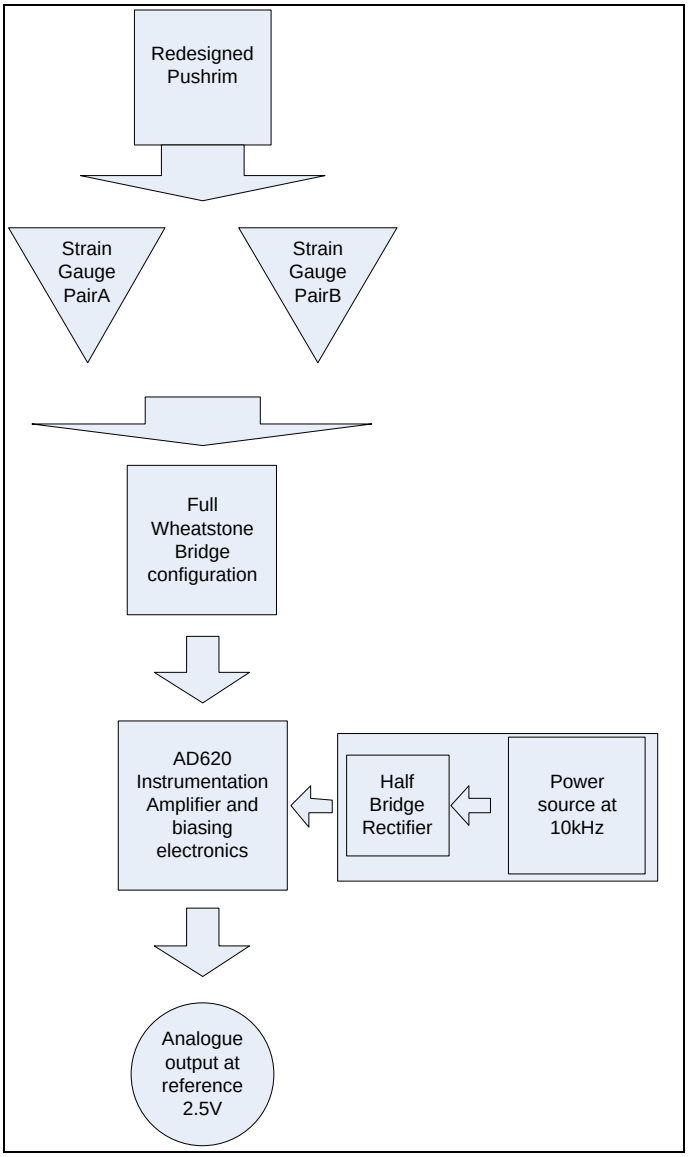

Figure 25: Measurement system block diagram

The second stage of the circuit design including the Wheatstone bridge and the instrumentation amplifier (AD620) can be seen in figure 26 below. The facility for two tuning resistors was included into the design to allow for balancing the Wheatstone bridge. This was in the event of slight differences in the mechanical fixing of the strain gauges, onto the redesigned iron struts supporting the pushrims. The option of connecting a tuning POT into the Wheatstone bridge was designed so to allow for the correct value of tuning resistors to be put into the Wheatstone bridge configuration. The POT was placed into the circuit and tuned until the output of the bridge was equal, it was then removed and the resistance was measured. The measured value of the POT was used to choose a resistor closest to this value, and

then placing this in the bridge. This ensured correct balance on the outputs of the Wheatstone bridge.

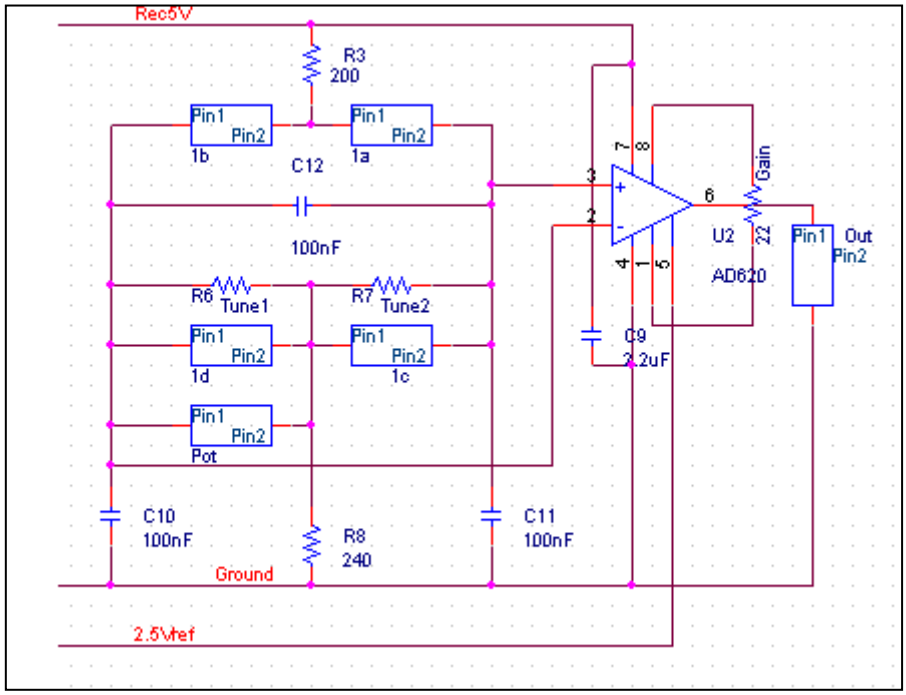

Figure 26: The second stage of the measurement designed circuitry

The inclusion of resistors R3 and R8 reduced the overall current flow through the Wheatstone bridge and also set the boundaries for the upper and lower voltage thresholds of the outputs. A reference voltage of 2.5V was set on the AD620 so to allow the maximum amount of voltage swing from 0V to 5V around the 2.5V reference when measuring the force with the strain gauges. This was accomplished by using a resistor pair and a LED pair in a voltage divider configuration.

4.3.4 Measurement electronics power stage

The first stage of the design incorporated the electronics for a stable power source for the Wheatstone bridge and for the stable 2.5V reference for the AD620 instrumentation amplifier. The rectification electronics was also included to rectify the voltage set wirelessly over the magnetic coils. This will be explained in detail further on in this study.

The figure (Figure 27) below illustrates the first version of the complete printed circuit board, designed and developed for this specific application. The PC board design allowed for minimal noise interference ensuring a stable platform for the measuring system. The inclusion of surface mounted components assisted with the stability of the circuitry.

Figure 27: Measurement electronics PC board

The complete design allowed for sufficient force measurement by the electronics. A stable 2.5V reference voltage was produced which was sufficiently temperature stable.

Many experiments were performed on the newly designed force measurement electronics, by visually monitoring the voltage output of the AD620 in proportion to the input strain onto the pushrim by the user. The aim of this project was to ensure that the voltage remained at 2.5V when no force was applied, and with both positive and negative force applied a sufficient change of voltage, either towards or a maximum of 5V output for the forward applied force, or towards 0V or a minimum of 0V for a reverse force applied. With additional time and budget the force measurements could be recorded and published, but the visual results sufficed for this level of project.

4.4 Wheelchair electric assist conclusion

The study set out to investigate the mechanical modification of a standard locally manufactured manual wheelchair to an electric unit. Hub motors were chosen as the primary power source due to their high output power and compact design.
Through various redesigns a prototype electric wheelchair was produced by modifying and existing manual wheelchair. The need for an electric assist type option became apparent due to the number of disease weakened persons in Southern Africa. A design decision was taken to experiment with various options for measuring the forces applied by wheelchair users on the pushrims of the wheelchair and proportionally assisting the user via the wireless signal transfer from the wheels pushrims to the static wheelchair frame and motors.

A prototype was successfully designed and built that incorporated force measurement via strain gauges on the support struts of the pushrims. Advanced electronics were designed ensuring that accurate and stable force measurement was achieved. The electronics designed were used in two different applications in this project, namely the force measurement by the user on the pushrims and the design of a static joy stick for manual manoeuvring of the individual wheelchair wheels. The joystick design considerations will be discussed next in this paper followed by the wireless power and signal transfer techniques experimented on.

CHAPTER 5
Joystick design and construction

5.1 Static joystick design introduction

A pair of joysticks were developed for the control of the two hub and wheel assemblies. The joystick design accommodated a two directional operation, allowing for forward, backward, left and right movement by the user either powering the left or right more for the turning actions.

The joystick incorporated a solid state design using a pair of strain gauges mounted onto a piece of spring steel. This allowed for proportional force vs. speed and direction control. The complete design will be covered in this chapter.

'Force' joysticks in industry are widely available and reasonably cost effective, questioning the reasoning behind the design of this joystick. The aim of the joystick development was to prove that the developed force measurement versus proportional output voltage techniques could be utilised in many applications. The reasons for designing such a joystick proved that this prototype was exceptionally cheap and simple to construct. It only utilises a single axis, opposed to the commercially available joysticks using two axis's, reducing the costs dramatically. The electronics ulitised in this joystick are identical to what was used to measure force on the wheelchairs pushrims, justifying the advantages of this design.

5.2 Joystick design considerations

Two 120Ω, 0.3% tolerance strain gauges were fixed to a piece of spring steel, mirroring each other. The bottom of the spring steel was bent so to allow for fixing on a satisfactory base. The design is illustrated in Figure 28 and 29 below. These were similar strain gauges and configurations used for the measurement stage described earlier.

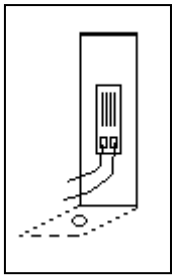

Figure 28: Spring steel bend at 90 degrees with two strain gauges mounted on each side

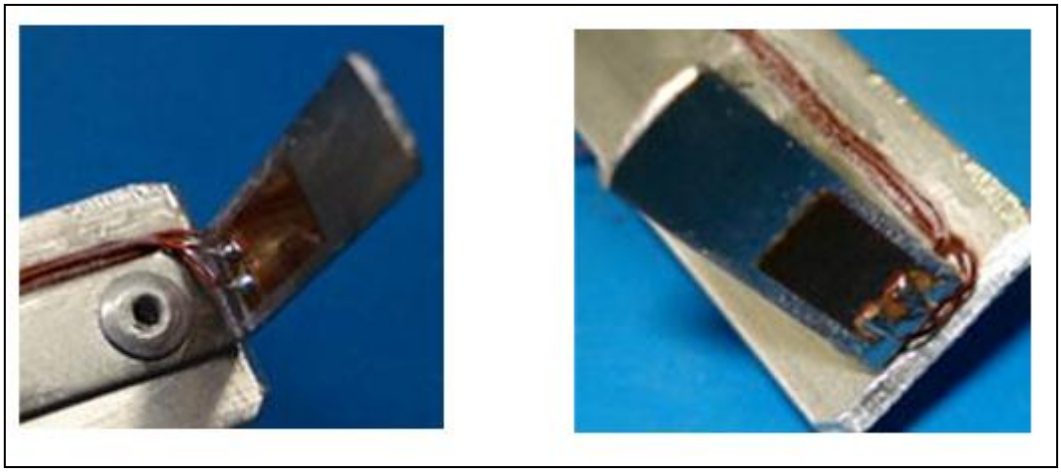

Figure 29: Prototype joystick assemblies constructed out of spring steel while mounted on aluminium angel iron

The strain gauges were connected in a similar Wheatstone bridge configuration as described before, with the two strain gauges forming the one half of the bridge while two dummy 120Ω resistors forming the other half of the Wheatstone bridge. The similar configuration of the design is shown in figure 30 below.

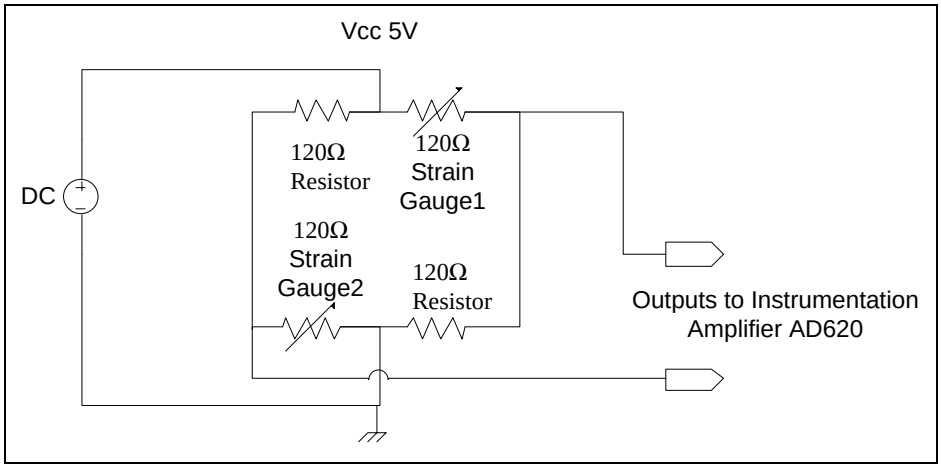

Figure 30: Two strain gauges and two dummy resistors in the Wheatstone bridge configuration

As described before under no-load conditions the Wheatstone bridge was balanced and the potential difference of 0V was measured at the output. Once a force was applied to the system the balance of the system changed and changed the output voltage proportional to the force applied. A block diagram shown in figure 31 details the joystick design follows below.

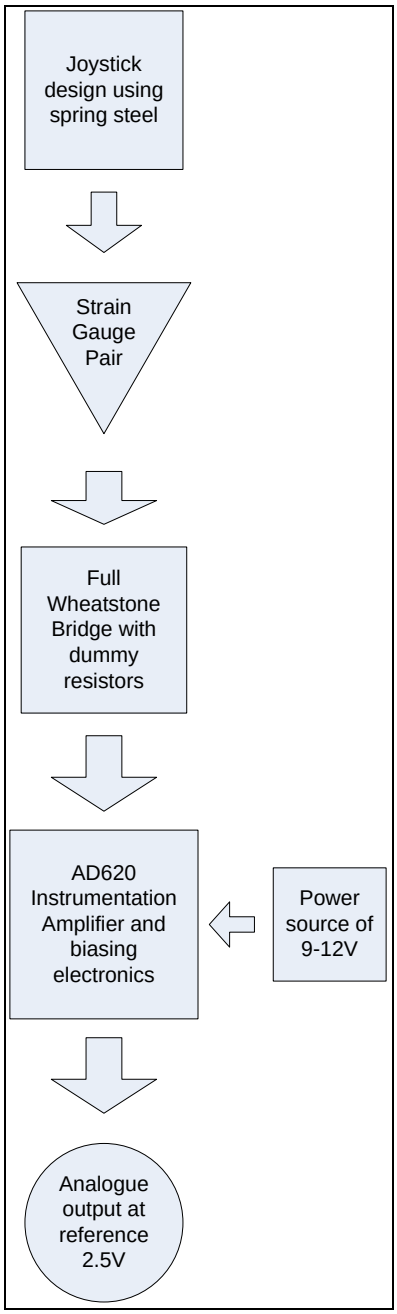

Figure 31: Joystick operational block diagram

The second stage of the circuit resembled the measurement design stage detailed before including the Wheatstone bridge, instrumentation amplifier (AD620) and tuning facilities shown before.

The First stage of the design incorporated the similar voltage source and referencing power unit for driving the Wheatstone bridge configuration detailed before, including:

- Direct Current connectors for the operation of the joystick.
- The stable 5V regulator supplying the Bridge
- The voltage divider incorporating the LED's and capacitors to supply the stable 2.5V reference for the AD620.

Note: This design was mirrored for both the joystick and pushrim force measurement system, with the only difference being the rectification electronics used for rectifying the 13 kHz signal sent wirelessly between the frame and the independent wheel, the full detail will follow.

The prototype was fixed into a plastic housing which can be seen in figure 32 below.

The first image shows the top view, with the joystick arm protruding out of it, the penetration shown acts as a mechanical stopper ensuring a user doesn't overdrive the joystick in either the front or backwards positions.

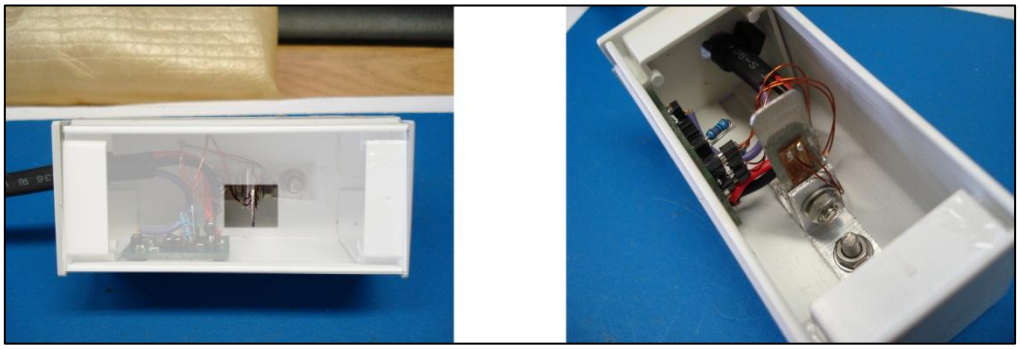

Figure 32: Two different views of the prototype joystick housing made out of PVC plastic

The two joysticks were mounted on the two support arms of the wheelchair frame so to allow the user easy access on either side of the chair.

5.3 Joystick design conclusion

A static type joystick design as described and built in this chapter had practical applications as users with severe neuro-muscular disorders like Cerebral Palsy and Parkinson's disease could operate this electric wheelchair due to the simple two quadrat application of these joysticks. A standard four quadrant wheelchair joystick allows for free motion through all quadrants, where the static type joystick only allows for a forward and backward motion.

The output proportional voltage to user input could be interpreted by the hub motor controllers ensuring a proportional thrust is applied by either one of the hub motor and wheel assemblies.

The joystick design was considered via considerations between the researcher and the supervisory body at the CIR (CPUT) and thus influenced the following methods of research trial and error. Without time constrains and limited budgets the method of calculating the shear bending moments of the spring steal could have been achieved, allowing for a possible improvement of strain gauge choice for this portion of the project.

CHAPTER 6
Wireless power generation

6.1 Wireless power generation Introduction

The thesis discussed the redesign of the wheelchair accommodating the electric motors for propulsion and the detailed discussion surrounding the force measurement on the wheelchair pushrims fixed on the wheels for the electric assist option. The force measurement electronics comprised of a resistive strain gauge Wheatstone bridge topology with carefully designed comparative electronics responsible for giving a proportional referenced output voltage, in relation to the applied force on the pushrims, by a user. The nature of the system meant that the measurement electronics were situated on the moving wheels of the wheelchair, where the pushrims were mounted. Due to the resistive nature of the measurement electronics and the low resistances of the strain gauges, the electronics required about 35mA at 6-7 VDC to function. Figure 33 below depicts the circuit configuration of the strain gauges with current limiting and voltage capping resistors explained in detail in Chapter 4. The current required for this circuit shows that the minimum allowable current to be 9mA.

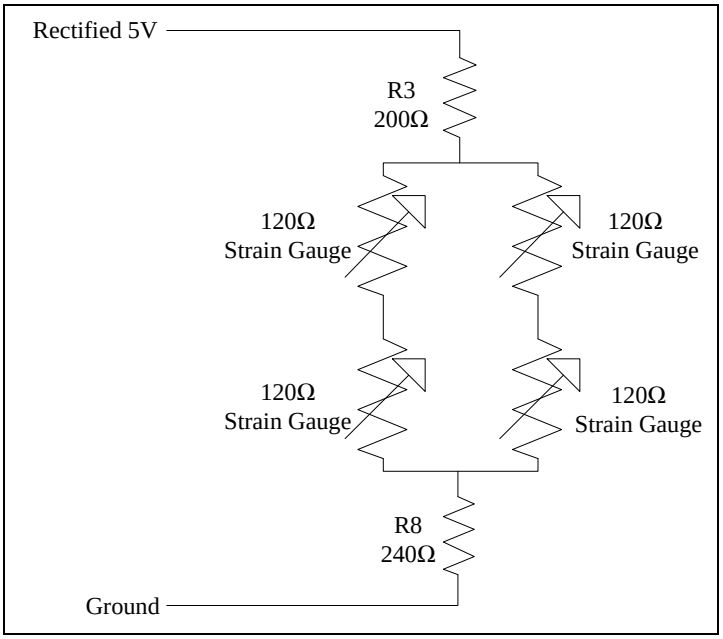

Figure 33: Wheatstone bridge with current regulating and voltage capping/current regulating resistors, extracted from the measurement electronic circuit

Included in the overall power requirement of the system was for the voltage regulation, voltage referencing (2.5V), AD620 instrumentation amplifier and the

wireless signal transfer circuitry that will be explained in detail further on. The total power required for the measurement electronics separated by the rotating barrier was 35mA at a minimum voltage between 6 – 7V, overcoming the minimum voltage requirement of 5V for the regulator. The measurement electronics prototype supply current was measured to determine the overall power requirements noted. The reasonably high power requirement for the measurement electronics highlighted the need for power source research. Batteries are the common independent power source unit utilised in most industry applications with Radio Frequency power transfer, influencing the following research.

6.2 Power source considerations

6.2.1 Radio Frequency power transfer option

The most common way for electronics to communicate with each other is via the method of transmitting and receiving high frequency radio waves. This RF (Radio Frequency) method for transmission of information has been common place for over a century. A consideration was made to adopt this method for the power transmission from the frame of the wheelchair to the measurement electronics on the rotating wheel.

The problem with RF wireless power transfer was that the efficiencies of the system needed to be higher than what was available, ensuring that most of the energy expelled by the transmitting circuitry be received by the receiver. When radio waves are transmitted they get expelled from the transmitter's antenna omni-directionally, this is dictated by the Rayleigh Criterion [Williams, Carter 2009] which states that any radio wave will spread and become weaker over distance. This fact highlighted that this RF solution for power transfer was too inefficient for this application, where the receiving power requirement was reasonably high. Other RF techniques had proved better in efficiency ratings like microwave beaming, but these were never considered nor researched as practically the costs and complexities of these systems were out of scope. With additional time and budget additional RF power transfer techniques could be studied and documented, resulting in other possible solutions.

6.2.2 Battery operated power source option

Research was done on standard SLA (Sealed Lead Acid) batteries as they were rechargeable and reasonably cost effective. A 6V 0.5 Ah SLA battery was considered due to the size and cost. Larger capacity batteries became bulky and the prices increased dramatically. A scaled 1:1 ratio figure of the dimensions of a typical 6V 0.5 Ah SLA battery is shown below, indicating the actual size of a battery. These batteries retail at around R160.00 as indicated by [Robot MarketPlace (2010)] online store.

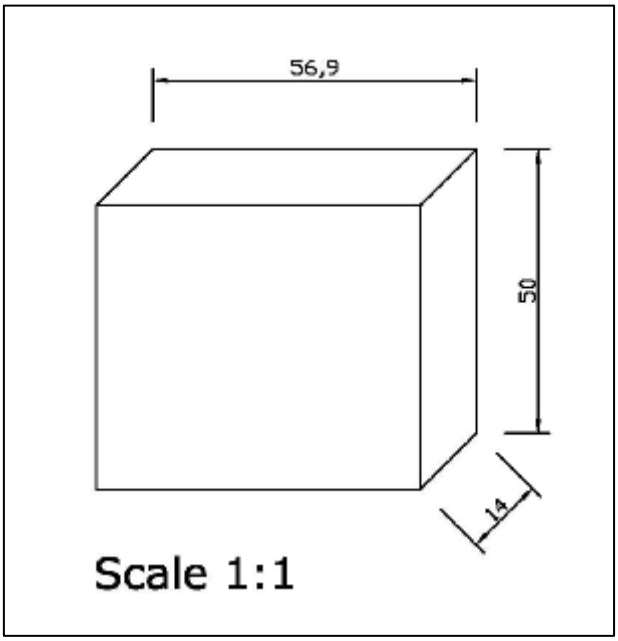

Figure 34: Actual size of a typical 6V 0.5Ah SLA battery

A simple calculation, shown below indicates that at the required power of 35mA at 6 – 7V the measurement electronics would last 14.29 hours.

$$Running\ Hours = \frac{0.5A}{35mA} \text{ (equation 7)}$$

$$Running\ Hours = \mathbf{14.29hours}$$

This seemed acceptable but the bulky design of the batteries posed problems for mounting them directly onto the independently spinning wheels. The wheelchair as a whole required battery charging, so introducing a secondary set of batteries for charging seemed unpractical, considering that the primary users for this type of electric wheelchair lived in the rural areas of South Africa, where charging maybe an

issue. Complicating the operations (charging) of this wheelchair was not an option. This highlighted a power source requirement that did not require any charging and capable of supplying continuous power of 35mA at 6 – 7V.

In Chapter 2 the slip ring and transformer coupling power transfer methods were discussed in detail. These technologies were strongly considered as both had the potential to supply the required power over the rotating air barrier continuously, due to the high efficiencies of these electrical conduction methods.

6.2.3 Slip Ring power transfer option

A slip ring is an electric type connector developed to transfer current or signals from a stationary body into a rotating device. Typically it comprises of a stationary graphite or metal contactor which rubs on the outside diameter of a rotating metal ring. As the metal ring rotates, the electrical current conducts via the fixed brush onto this metal ring enabling a path for the current to flow between the fixed brush and the rotating ring. Additional ring and brush assemblies could be mounted along the rotating axis to provide additional electric circuits (Mercotac, Inc, 2011).
In conclusion the slip ring method for current conduction to the measurement electronics across the rotating barrier posed possible problems such as:

- Slip Ring connectors by nature have moving parts brushing up against each other, these over time will ware away causing connection problems.
- Slip Rings operating in dirty and dusty conditions maybe prone to particles getting lodged between the brushes and ring, causing further connection problems.

Due to these issues slip rings were not considered as the power transfer method on this electric wheelchair project, the practical solution was to utilise the completely wireless power transfer solution adopted by transformers with airgaps. The flux coupling method with prototype development is described further.

6.3 Transformer coupling and current transfer

Faraday's law states that a voltage is induced around a loop of wire when a time-varying magnetic field passes through the surface of the closed path (Drewniak, 2011). This fundamental principle is the basis of the wireless power transfer system developed for the wheelchair. The principle of a transformer is based on the magnetic field generation around a coil of wire when an electric current is passed through it and that a changing magnetic field within a coil of wire induces a voltage across the ends. By varying the current in the primary coil of the transformer similarly alters the magnetic flux that it produces, inducing a proportional voltage in the secondary coil. A typical transformer model is shown in figure 35 below.

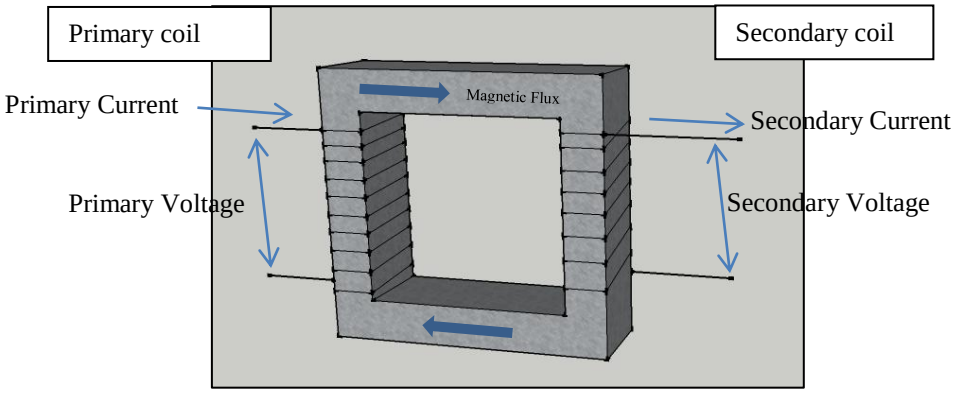

Figure 35: Typical transformer model

The model illustrates the basic theory of how the magnetic flux flows through the transformer core from the primary windings to the secondary. A proportional voltage in the secondary winding turns is produced at the secondary output.

This basic model formed the foundation of the wireless power transfer principles adopted in the electric wheelchair project. What differed was that a portion of the transformer core was an air gap where the magnetic flux passed through, inducing a voltage on the secondary. This is shown in figure 36 below. The transformer type power transfer design and prototype is discussed further in this paper.

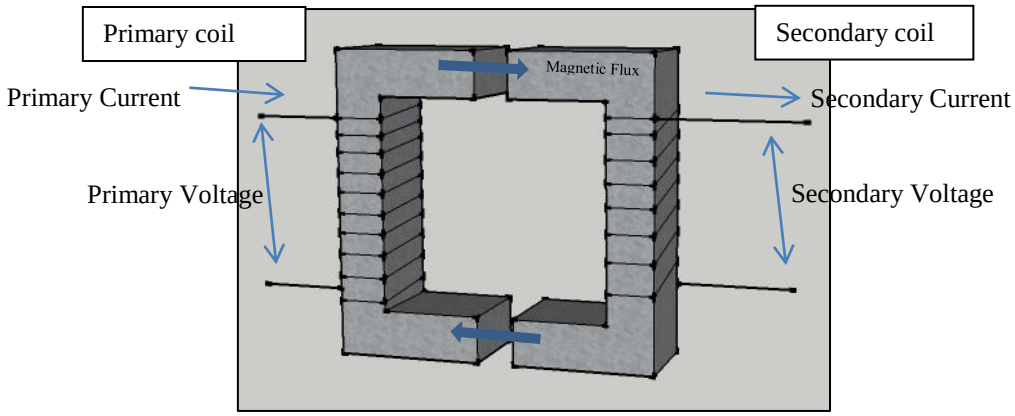

Figure 36: Typical transformer model with an airgap

6.3.1 Mechanical design with considerations

The research into the wireless power transfer led to the design decision of utilising the transformer flux coupling method via a core airgap. Further considerations were around the physical construction of the transformer type primary and secondary coils, while considering a fixing technique onto the wheelchairs redesigned frame and rotating hub motor.

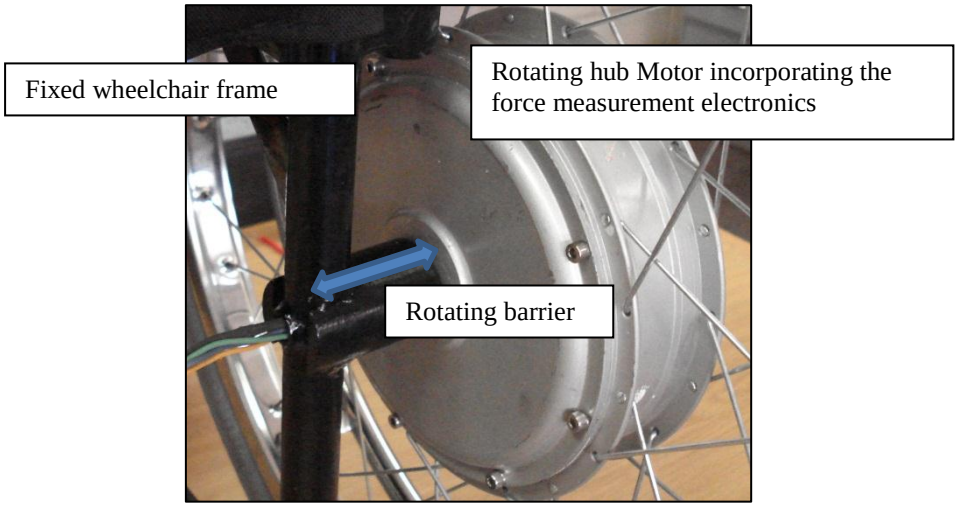

Figure 37: Illustration of the redesigned wheelchair frame, showing the rotating barrier where the wireless power transfer was required

Figure 37 illustrates and describes the challenge of transferring power from the fixed wheelchair frame to the rotating hub and wheel assembly. A decision was made to design and build the primary and secondary coils into matching circular shapes allowing the primary to be mounted around the new hub shaft mounting bracket (hub)

and the secondary to be fixed onto the inner face of the rotating hub motor. The described design strategy is illustrated below in figure 38.

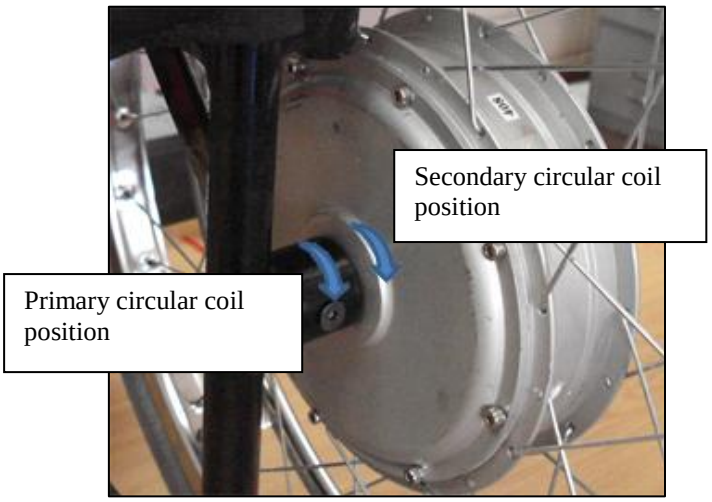

Figure 38: The primary and secondary mounting positions

Through experimentation the following design and prototype manufacturing techniques were adopted.

6.3.2 Primary and Secondary coil design

Research was done on mounting a coil on the wheel and fixing a second coil on the frame. These two coils ran side-by-side, one being static on the frame and the other moving with the wheel. These acted as the primary and secondary coils of a transformer style generator, with a turn's ratio of 1 to 1. Two inner winding cores were machined out of nylon allowing for the transformer wire to be wound around it, these were then encased in a polymer mixture. A casting mould was machined out of aluminium, ensuring for precision casting of multiple coils with exact size matching. Iron filings were added to the polymer mix hoping for better flux coupling. The described components are illustrated in figure 39 below:

A – Machined Nylon inner core (stage 1)
B – Machined aluminium precision mould (stage 2)
C – Top view of the first phase polymer and iron filing mixture cast (stage 3 – result)
D – Bottom view of the polymer mixture cast showing the nylon inner core winding (stage 3 – result)

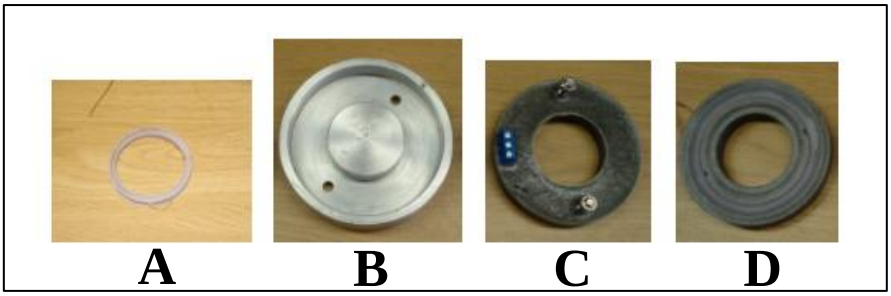

Figure 39: Illustrates the machined inner nylon core, aluminium mould, top and bottom view of the first prototype polymer and iron filing cast

The above illustrated casting process was adopted for all prototype primary and secondary coils in this project.

The primary and secondary cores flux coupling and voltage generation was tested by utilising a changing DC square wave from a function generator. The primary and secondary coils were held up against each other while the primary coil was excited by the changing DC voltage. A simple voltage rectification circuit was produced so to rectify the changing DC output voltage on the output of the secondary. The output was measured and the resulting voltage was checked to ensure it was adequate for use in this application.

6.3.3 Initial encased coil design considerations

The nylon inner cores for the primary and secondary were wound with a coated copper transformer wire at 0.5mm diameter at 60 turns cast in an iron filing and polymer mix, producing a transformer ratio of 1:1, this is shown in figure 40 below. The function generator was put onto the input of the primary coil with a changing 10V peak-to-peak square DC wave, the coils were held together and through simple rectification of the secondary changing output voltage the output was measured.

Figure 40: Initial nylon coil with 60 turns cast in the iron filing and polymer mixture

The result of this experiment showed that the 60 turn coil did not produce a high enough output voltage at the secondary coil. An output voltage of 2V was produced which did not allow for a suitable output voltage range. The required output voltage range as stated before in this dissertation, needed to be a minimum of 5V, referenced at 2.5V. Further experimentation was performed by changing the number of coil windings, recasting and retesting the outputs, further resulting in unusable output voltage ranges. The conclusion was that the initial prototype coil encased in the iron filing and polymer mixture did not produce sufficient flux coupling resulting in better transformer efficiencies and usable output voltages.

Thought went into producing a more efficient transformer, thus generating more power through higher transformer coupling efficiencies. Considering a standard transformer model illustrated earlier in this chapter highlighted the need to direct the flux via a medium between the primary and secondary coils. Transformers commonly utilise a standard laminated core material sandwiched together producing a path for the flux to travel.

The decision was made to construct a version of the prototype including the coil wound of similar 0.5mm diameter coated copper transformer winding wire with 15 turns and modify ‘over the shelf’ transformer laminations to generate a better flux coupling and higher transformer efficiencies, in the hope to produce the required output voltage range at the secondary output.

6.3.4 Final encased coil considerations

The purchased transformer laminations came in standard E shape which was modified into a U shape, allowing for mounting around the machined nylon core. Figure 41 shows the standard E shape lamination (A) and where they were cut producing the U shape lamination (B).

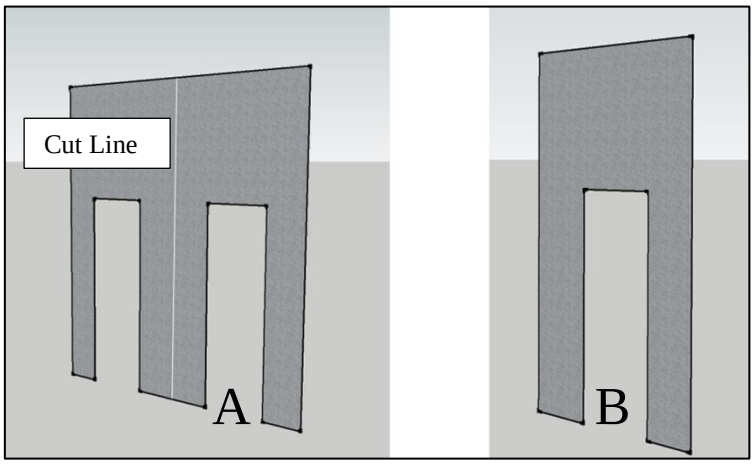

Figure 41: A - Illustrating the purchased E shape transformer laminations, B - illustrating the final prototype U shape lamination after modification

The prototype design and manufacture is best explained via illustrations and descriptions, following in sequence as detailed below.

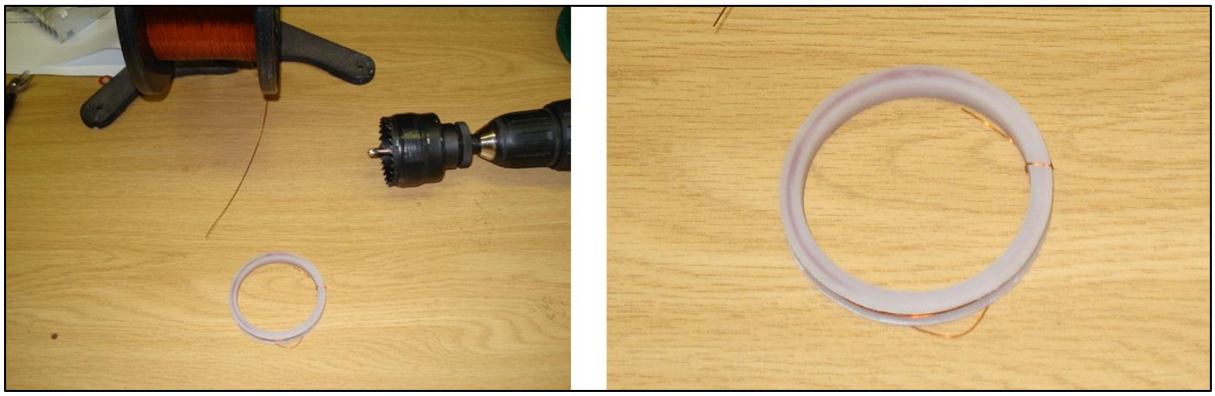

Figure 42: The first stage of the coil prototype manufacture. A nylon inner winding hub was machined to support the 0.5mm diameter coated copper transformer winding wire. The copper wire was wound to 15 turns using a cordless drill

Figure 42 illustrates how the inner nylon machined core was wound with the 0.5mm diameter transformer wire using a cordless hand drill. The decision was taken to wind

the coil to only 15 turns as the expected flux coupling efficiency would be higher, requiring less primary winding coils. The design techniques were considered via trial and error, until the desired results were achieved.

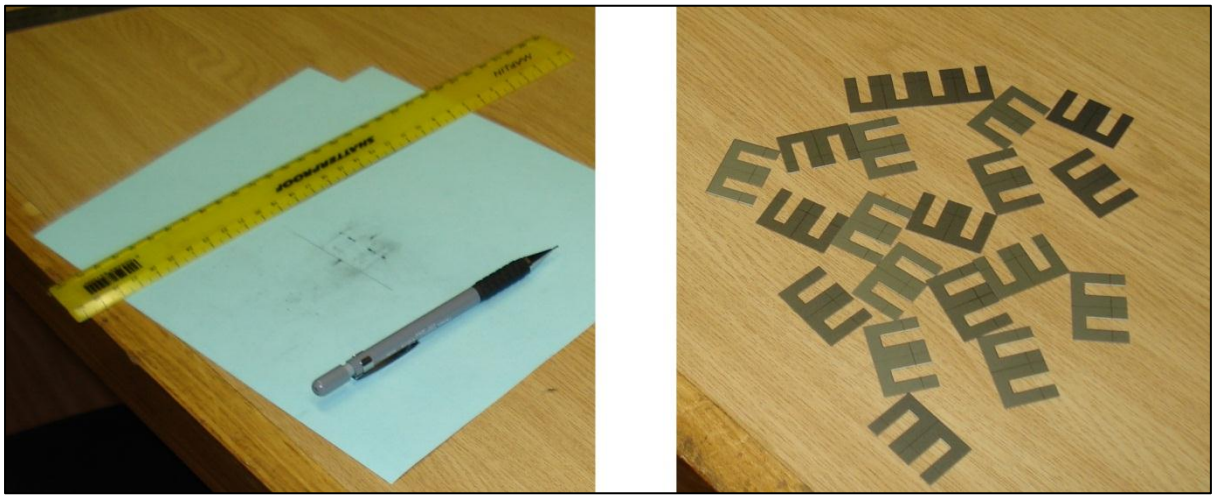

Figure 43: The second stage of the coil prototype manufacture. Standard transformer laminations were manually measured and cut to size using a pair of tin snips

As described earlier the E-shape transformer laminations were modified creating a C-shape lamination which could fit snugly over the machined and wound inner nylon core. The forecasted assembly was to create a primary and secondary transformer core incorporating an airgap as earlier described, the transformer model detailing the wound primary and secondary cores with the appropriate airgap.

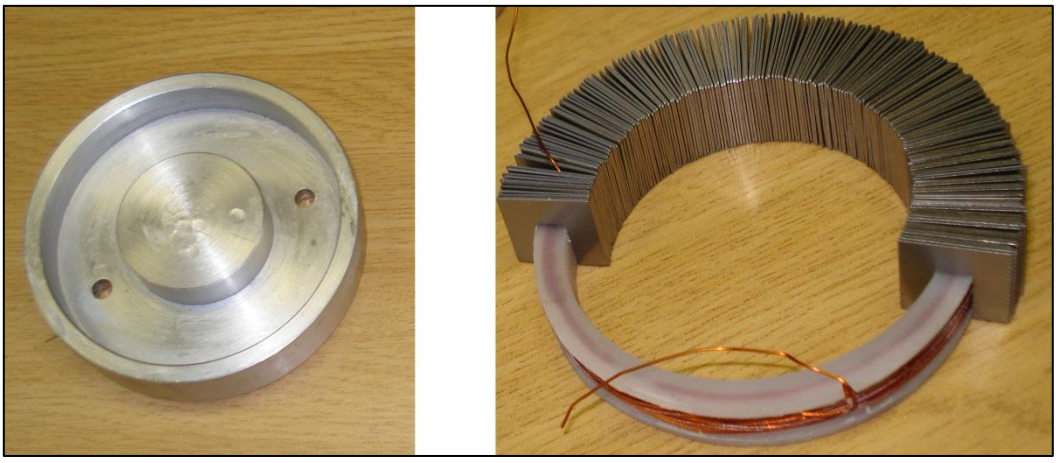

Figure 44: Third stage, the cut transformer laminations and inner coil winding assembly. The laminations were modified to best fit the inner transformer core

Figure 44 shows the modified transformer laminations and inner nylon wound core assembly progress. The idea was to surround the entire nylon core with the C-shaped laminations while ensuring the entire internal assembly could still fit within the machined aluminium cast. The assembly would be cast solid in a similar polymer compound utilised earlier.

The transformer model with airgap described earlier indicated how the flux gets directed around the transformer core material, over the airgap. The idea for this stage of the prototype development was to mimic the transformer model many times over, with multiple C-shaped laminations packed side-by-side continuously around the circular core, in the hope for higher efficiencies between the primary and secondary cores surrounded by C-shaped laminations.

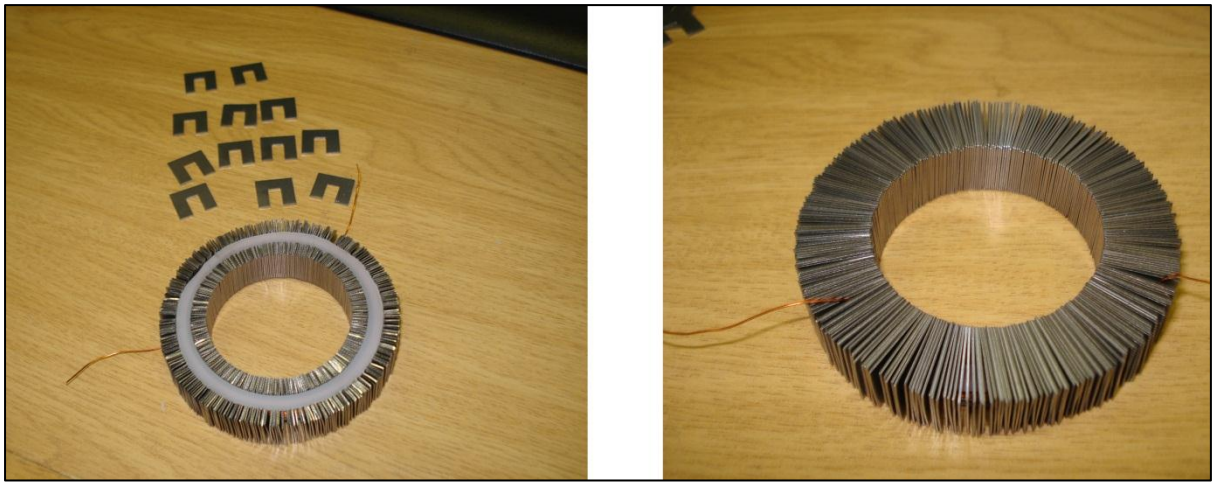

Figure 45: Final stages of assembly. The laminations were placed as tightly on the inner core as possible. The final lamination count was 250

The completely surrounded inner core with laminations is illustrated in figure 45 above. The final lamination count for both the primary and similar secondary cores was 250.

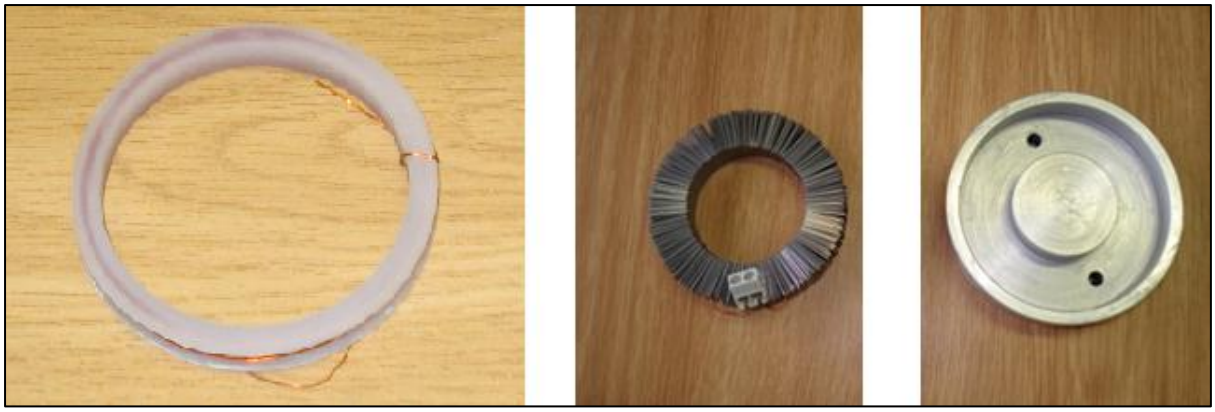

Figure 46: The casting process of the inner copper winding core with laminations, before a pure polymer was poured into the mould

The fully populated core laminated inner coil was now ready for final assembly and casting with the pure polymer mix. The previous core design was cast in a polymer and iron filing compound, in hope to assist with the flux coupling. This resulted in inadequate output voltages due to below expected efficiencies and flux coupling when the appropriate tests were performed. The following prototype utilised transformer core laminations assisting with directing the flux from the primary to secondary coils, eliminating the need for the iron filings in the compound.

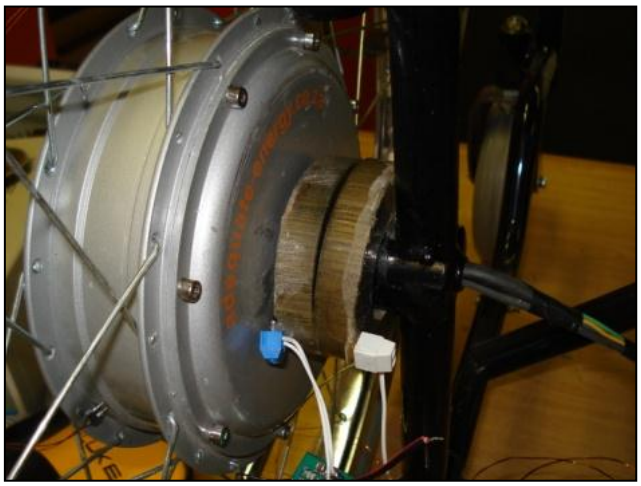

Figure 47: Depicts the final prototype. The primary and secondary transformer generator coils are shown mounted onto the fixed wheelchair frame and moving hub and wheel assembly. The final fixed distance from primary to secondary coils was 1mm

The final prototyped primary and secondary laminated cast cores are shown in figure 47. The earlier described mounting technique is seen with the primary coil assembly fixed onto the static wheelchair frame, with the secondary fixed onto the rotating face of the hub motor. An airgap of 1mm was set between the two coils.

On testing the final prototype with the input function generator set at a 10V peak-to-peak square wave while a manual frequency sweep was performed. The output voltage, after the described rectification was measured while the primary and secondary coils were held at 1mm apart. The resulting output voltage at the frequency range of between 7 kHz and 15 kHz fell within the required range of above 5V. This became the final prototype coil design for both the primary and secondary.

The research following discusses the development of the primary coils square wave generator with the secondary coils rectification electronics. Before the development of the oscillator circuitry the combined primary and secondary coils natural resonance was required. Oscillating coils at resonance improves the efficiencies dramatically enabling higher power generation on the secondary coil. The following measurements and calculations were utilised in determining the combined primary and secondary coils natural resonant frequency.

6.4 Combined Primary and Secondary coil resonance frequency measurements and calculations

To maximise the transformer coil characteristics at a turns ratio of 1:1, the decision was made to oscillate the primary and secondary transformer coils at near resonance. This would allow for even greater power transfer and generation at the secondary.

Transformer coil frequency calculations:
Primary transformer coil: 15 turns
Measured resistance: R = 0.72 ohms
Measured individual inductance: L1 = 62.57uH

Secondary transformer coil: 15 turns
Measured resistance: R = 0.72 ohms
Measured individual inductance: L2 = 62.87uH
The combined measured inductance while the two coils were mounted onto wheelchair frame and hub wheel assembly, with **no** air gap: L1 + L2 = 140uH.
The combine measured inductance with the primary and secondary coils mounted onto the frame with an air gap of **1mm**: L1 + L2 = 98uH.

A 2.2uF capacitor was used to calculate the combined resonance frequency of the primary and secondary transformer generator coils.

$$f = \frac{1}{2\pi\sqrt{LC}}$$ (equation 8)

The calculated resonance frequency of the combined coils **without** an air gap, mounted onto the wheelchair frame: **9 kHz**

The final working calculated resonance frequency of the combined coils with a **1mm** air gap, mounted onto the wheelchair frame: **10 kHz**

Through experimentation and measuring the output voltage and current of the secondary transformer generator coil, the final square wave frequency required was designed at 13 kHz. This was 4 kHz above the combined resonance of the primary and secondary coils, giving the desired 6-7V at 35mA, which will be discussed further on.

6.5 Primary coil square wave generator

A consideration was made into square wave oscillator circuits with the simple inverter type oscillator standing out as the usable option. The decision was taken to utilise an efficient and high power MOSFET driver as the inverter for the oscillator. The MAXIM supplied MAX5048 high-speed MOSFET driver was chosen for the oscillator circuit due to its high sinking/sourcing current ratings of 7.6A and 1.3A respectively. The MOSFET driver had inverting and non-inverting inputs allowing for the necessary flexibility required for designing the square wave oscillator. The devise also boasted a single power supply requirement making it the ideal component in the oscillator design ensuring a high current positive changing DC output with an operating voltage between +4V and +12.6V (MAXIM Integrated Products, 2005).

6.5.1 Square wave oscillator design considerations

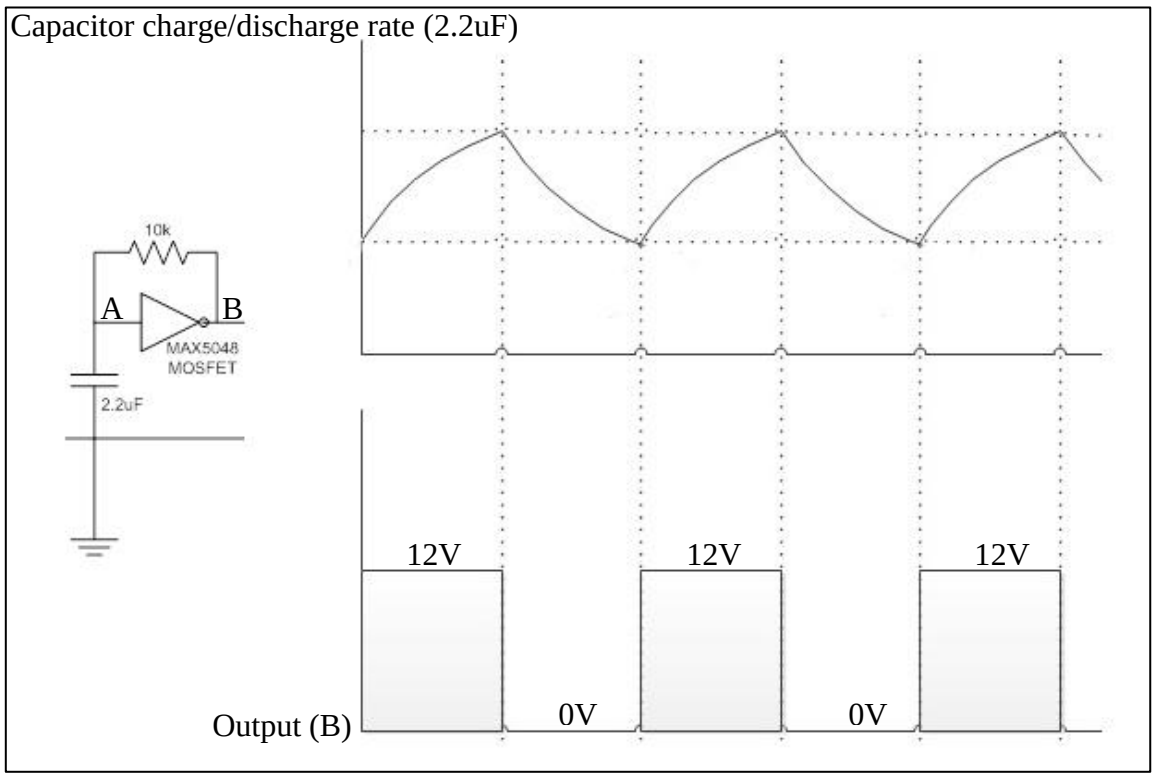

Figure 48: The inverter (MOSFET) square wave oscillator operational diagram

On initial powering up of the circuit the voltage over the capacitor (2.2uF) remains at 0V setting the voltage at the input (A) of the MOSFET driver at 0V. The MOSFET acts as an inverter so the output (B) of the inverter is held at VCC (12V). The designed operating voltage of the oscillator circuit was set at 12V matching the Hub Motors operating voltage. When point B sets to 12V the capacitor (2.2uF) charges via the resistor (10k). Once the capacitor (2.2uF) reaches the fully charged voltage of 12V automatically the input (A) to the inverter sits at 12V, setting the output (B) to 0V. As the output (B) is now set to 0V the capacitor discharges through the resistor (R) until fully discharged making the voltage over it 0V again. The cycle then repeats with the charging and discharging of the capacitor setting the output of the inverter (MOSFET) between Hi and Low at a frequency dependant on the ratio of the capacitor (2.2uF) and the resistor (10k). This is displayed in figure 48 above.

6.5.2 Primary coil square wave oscillator final circuit and description

A low frequency square wave was generated, using a carefully configured high power MOSFET driver. This was fed into the primary coil. The coils were fixed with an air gap of 1mm between them.

The power required was 6-7V at 35mA, used by the measurement electronics. After a few iterations the above mentioned and illustrated prototype proved to be reliable and allowed for sufficient power generation of 35mA. The complete circuit design can be seen in figure 49 below.

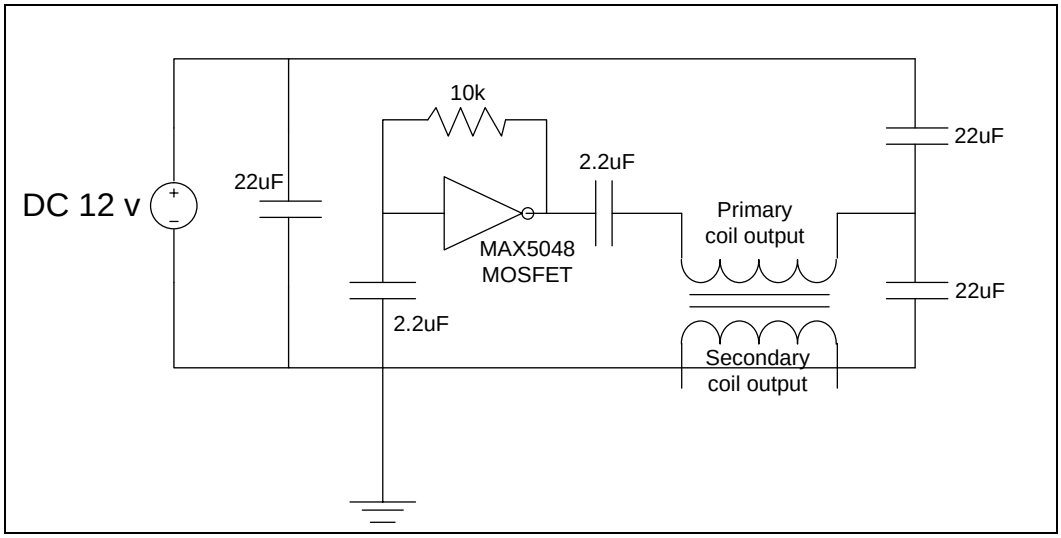

Figure 49: Final MOSFET square wave oscillator circuit

The MOSFET oscillator RC couple was set at 10k and 2.2uF respectively, which provided the required 13 kHz, 12V p-p square wave at the required 35mA. The two 22uF capacitors function as voltage stabilisers ensuring the oscillating output remains consistent.

6.6 Secondary coil, rectification and smoothing circuit considerations

The secondary receiving coil located on the rotating wheelchair wheel is described below. This includes the rectification, smoothing and reference voltage generation circuitry.

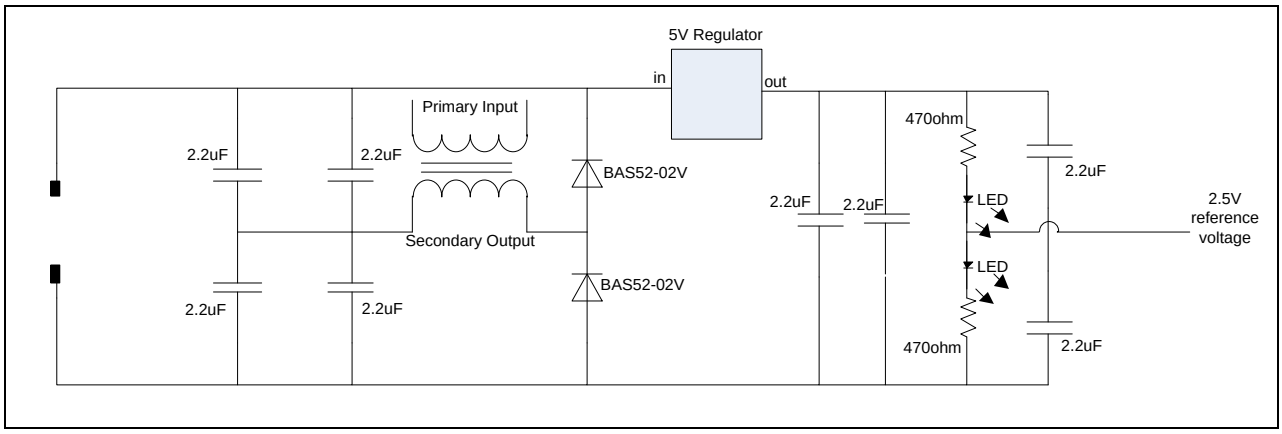

Figure 50: Rectification, regulation and referencing stage electronics

A full wave DC voltage rectifier was used to rectify the changing 12V DC square wave into usable 6-7V at 35mA. A highly accurate 5V voltage regulator was used to finally set the voltage at a stable 5V. The 5V rectifier powered the sensitive measurement electronics, so a stable supply was crucial. As before the stable 2.5V reference voltage was required for the instrumentation amplifier used in the measurement electronics. This was obtained by constructing a voltage divider with two LED's, which served as operational indicators.

6.7 Wireless power generation conclusion

The objective for this chapter was to discuss, design and build a method for wireless power generation on the rotating electric wheelchairs' wheels. This was required for powering the sensitive force measurement electronics responsible for the electric assist option discussed in detail earlier in this paper. The power requirement for the measurement electronics was reasonably high ruling out the discussed battery option. The slip ring method was not considered due to mechanical wear and tear and possible debris malfunction between the moving parts. The research led to utilising the common transformer flux coupling method across an airgap core for the primary to secondary energy transfer.

A number of prototype primary and secondary core designs were experimented on leading the study to modifying transformer type laminations to improve the unsatisfactory flux coupling. The final prototype incorporating multiple C-shaped transformer laminations cast around the coils mirroring a transformer theoretical

model discussed in this chapter. On final testing of the revised prototype the results seemed satisfactory achieving the required power generation of a 6-7V output at 35mA, across a 1mm airgap from the fixed wheelchair frame to the rotating wheel. The final chapter of this dissertation researches techniques of wireless force measurement signal transfer from the rotating wheel to the frame. Figure 51 below illustrates the prototype primary and secondary coils situated at 1mm apart.

Through trial and error research the transformer coupling system proved satisfactory. With additional time and funding further research could be achieved into prototype efficiencies and design problems. The final prototype developed in this thesis was sufficient for the level of project designed.

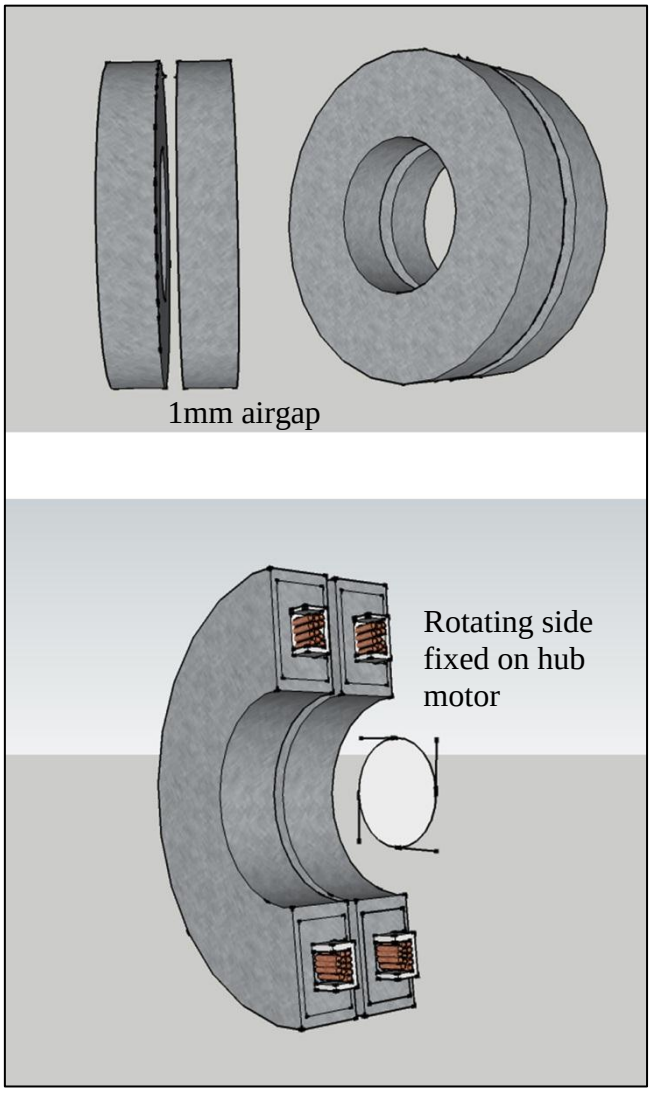

Figure 51: Digital illustration of the primary and secondary coils at 1mm apart

CHAPTER 7
Wireless measurement electronic signal transfer

7.1 Measurement electronics with wireless signal transfer Introduction

Previously in this study research and design was done on the power stage of the project incorporating electronics for a stable power source, wirelessly generated over the air barrier from the wheelchair frame to the rotating wheel. This was used to power the measurement Wheatstone bridge strain gauge configuration and supply a stable 2.5V reference, for the AD620 instrumentation amplifier.

As detailed before, the design incorporated two pairs of strain gauges, fixed on the iron support struts at 180° of each other on the wheelchairs pushrims. The final fixing strategy and wiring is illustrated in Figure 52 below.

Figure 52: Final prototype strain gauge setup for the user force measurement

The typical Wheatstone bridge configuration diagram is shown below and described earlier in chapter 4 of this paper.

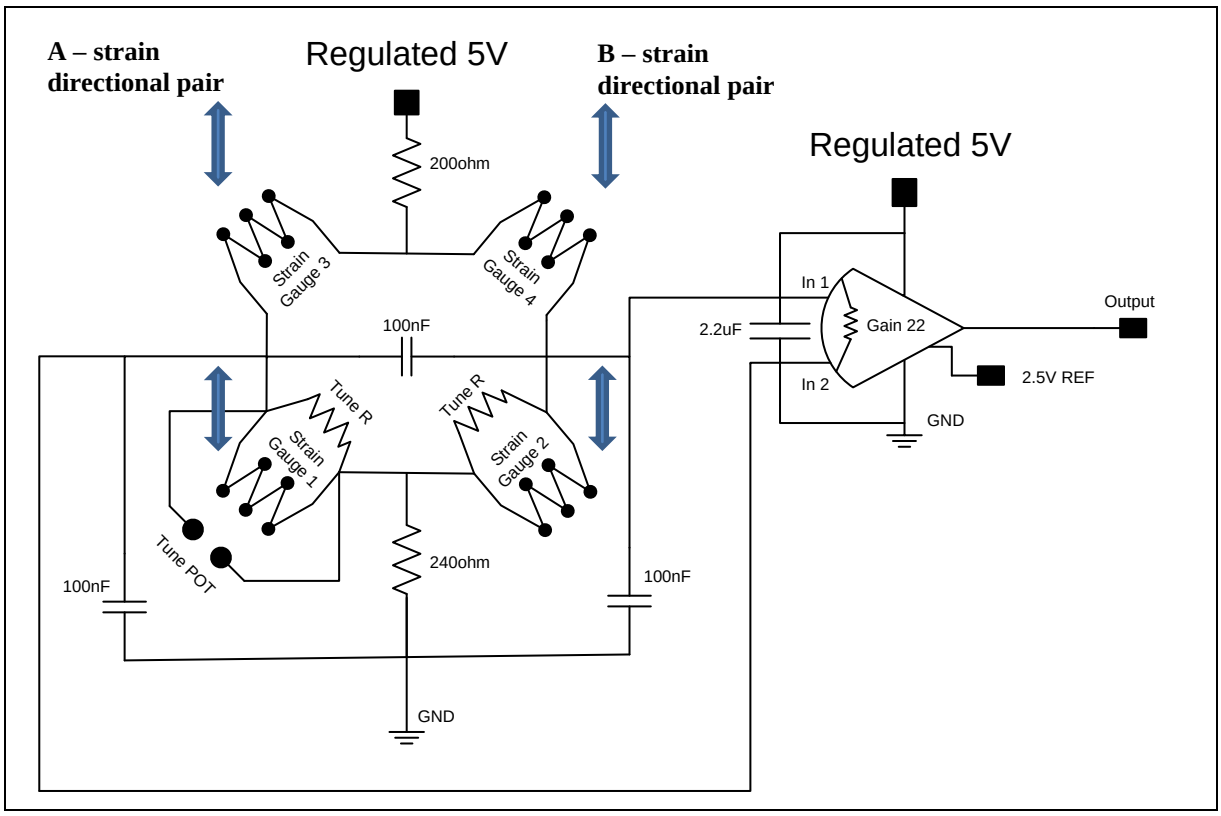

Figure 53: Typical Wheatstone bridge configuration

On the user applying a force in either of the directions, forward or backwards, the matched pair of 120Ω strain gauges change form in a similar fashion. The strain may either be compressive or tensile depending on the directional force applied by the user. The nature of a typical strain gauge allow for a resistance increase or decrease depending on the form distortion, as shown in figure 53 above (arrows). Expanding or stretching a strain gauge increases the resistance, while compressing or squeezing a strain gauge decreases the resistance. Chapter 4 detailed that once the user applies a force in a certain direction the balanced Wheatstone bridge detects a mechanical change and relays it into an electrical differential proportional voltage. This small voltage difference is detected by the sensitive instrumentation amplifier, referenced at 2.5V. The proportional applied user force translates to a changing voltage around 2.5V. With no force applied the output voltage remains at 2.5V, with a resultant voltage change from 2.5V up to 5V when a force is applied in the one direction and a voltage change from 2.5V to 0V with the force is applied in the opposite direction.

This proportional changing force dependent DC voltage was required to proportionally propel the individual hub motors situated on the wheelchair frame. With an increase of force in one direction the hub motors were required to reply with

a proportional mechanical force allowing for the force measurement and electric mobility assisted option, falling in line with the objectives of this project. A further objective of this project was to achieve reverse breaking when a user was running down an incline with the wheelchair. When the user applied a force in the opposite direction as to where he may be rolling the hub motors needed to apply a force to slow or even stop the electric wheelchair proportionally. These two primary functions of the wheelchair depended on the proportional analogue voltage being available on the fixed wheelchair frame for interpretation by the hub motors drive controllers.

The analogue signal similarly to the power generation discussed earlier, needed to be wirelessly transferred from the rotating wheel over the air barrier to the fixed wheelchair frame. A common industry standard signal transfer method adopted was to utilise a RF (Radio Frequency) method for digital signal transfer.

7.2 Wireless signal transfer considerations

7.2.1 RF signal transfer method considerations

As discussed in Chapter 6, the RF signal transfer method was also considered as a possible option for wireless power generation for the measurement electronics on the rotating wheel via the airgap. This was not considered as the final solution due to RF inefficiencies versus costs and complexity to power the components on the receiving rotating wheels. However the RF signal transfer method was considered as an option for wirelessly transferring the measurement circuitries proportional force, to output analogue signal from the wheel to the frame, as there was no high power application required.

As studied the analogue changing signal, referenced at 2.5V was required at the wheelchair frame for interpretation by the hub motor controllers, producing a proportional force to the mechanical force applied by the user on the pushrims. The objective was that the immediate force applied by the user required an instantaneous and proportional force reply by the hub motors, highlighting the need for a high resolution real time signal available at the wheelchair frame. Digital RF signals break an analogue signal down into data bits. These data bits are transmitted via an antenna

by oscillations of this signal. Depending on the accuracy required at the receiving end of the circuit determines the number of bits sent at a time, representing the analogue signal. So if the requirement was for a better resolution, a higher bit rate was required.

Discussions with some electronic specialists from a Cape Town company called RF Design highlighted that an RF method for wireless signal transfer of the changing analogue signal, would require electronics capable of very high accuracies. In conclusion this was achievable but RF electronics operating at such high accuracies was expensive and added design complexities which fell out of project scope. The primary goal of this project was ensuring the overall project costs remained low and simple, as the target market were the poorer communities of Southern Africa, ruling out the RF method for the wireless measurement signal transfer from the rotating wheel to the fixed wheelchair frame.

7.2.2 Tuned circuit wireless power transfer consideration

As previously detailed in this project a prototype wireless power generator was designed and built utilising the method of transformer flux coupling, with the primary input coil resonating near the combined natural resonance frequency and rectifying the secondary output into a usable high powered output voltage and current. This successful design influenced further research into similarly transferring the output measurement signal from the rotating wheels of the wheelchair to the frame.

7.3 Signal transfer using a parallel resonant circuit

Research was done on utilising the analogue signal to reference a VCO. The frequency of the VCO was set at 200 times the frequency of the power generation signal, which utilised the MOSFET driver oscillator. The large difference in frequency was required to eliminate any cross interference, between the power generation signal and the analogue signal described below. The roughly calculated frequency was set around 10MHz.

A second winding wound on the outside of the cast at a ratio of 1 to 2 was fixed so to produce a short range antenna. A 1 to 2 turns ratio was utilised to increase (double) the output voltage on the receiving frame antenna, this will be detailed further. The signal from the VCO was fed into the primary winding located on the moving wheel. This carrier signal was set at a frequency slightly below the resonant frequency of the combined coils with an air gap of 1mm. The carrier frequency was set at a level below the combined resonant frequency so to allow the full deviation of the FM signal while remaining on the lower slope of the band pass curve.

7.4 Balanced slope detector considerations

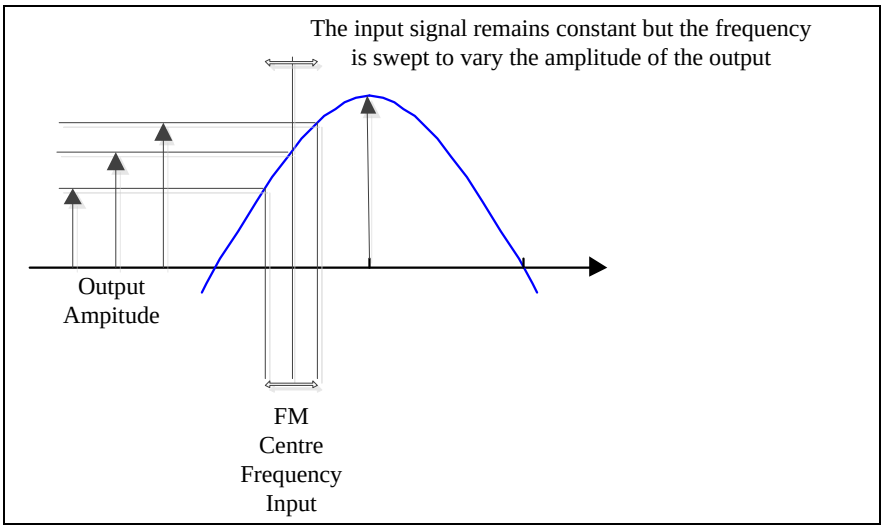

Figure 54: Typical balanced slope detector operation

When the FM carrier signal (see figure 54) was applied to the primary coil the output amplitude of the signal on the secondary coil fluctuates as the frequency moves further from or closer to the resonant frequency of both coils. The signal was read off the secondary winding, fixed on the static coil on the frame, using a diode detector. The diode detector acts as a rectifier, producing a DC voltage similar to the DC reference voltage supplied to the VCO. The final output amplitude was achieved by utilising a voltage doubler on the secondary coil output. Experimentation highlighted that the initial output voltages were unusable as they did not carry sufficient amplitude, resulting in the output voltages not matching the input voltage swing. The use of a 1 to 2 turns ratio of the coil windings with the output voltage doubler

achieved the desired output voltage. The detailed design of this will be described further in this dissertation.

7.5 Frequency-in versus voltage considerations

The design incorporated a voltage controlled oscillator controlled by a fluctuating voltage around a reference voltage of 2.5V. The carrier frequency was determined by the reference voltage of 2.5V. This set the mid-range frequency on the primary coil to ensure that the varying frequency range remained on the lower slope of the band pass curve and allowing for sufficient frequency variation. The frequency variation on the primary coil determined the amplitude variation on the secondary with rectification electronics, producing the desired fluctuating DC output voltage, referenced at 2.5V.

The designed system required a mechanical input from the wheelchair user, in a forward or backward direction in relation to the wheel and pushrim. The mechanical force was measured by the sensitive measurement electronics detailed earlier to produce the fluctuating DC voltage referenced at 2.5V, no load. A user input in a forward direction would require the output voltage to vary from 2.5V up to the threshold of 5V, and a backwards input would require the output to vary from 2.5V to 0V.

Due to the unique design parameters the correct output voltage generated wirelessly was achieved by experimentation. Variations on electronic and mechanical component configurations were experimented upon until the ideal setup was achieved, with the desired outputs. The resonant frequency aimed at was 10MHz, so to allow the large difference in frequencies between the power generation low frequency waves. As mentioned this was to avoid any unnecessary cross interference between the signal and power generation waves. The initial component choices were determined by using the frequency of 10MHz.

7.6 Signal transfer coils combined calculations and considerations (First stage of experimentation)

A similar strategy was adopted for calculating the resonance as previously discussed in this dissertation.

Primary and secondary transformer coil ratios: 1 turn at 1:1

The combined measured inductance while the two coils were mounted onto a 1mm thick Perspex sheet, allowing **a 1mm** air gap: L1 + L2 = 768nH

A 330pF capacitor was used to calculate the combined resonant frequency of the primary and secondary signal transformer generator coils with the formula shown below.

$$f = \frac{1}{2\pi\sqrt{LC}} \text{ (equation 9)}$$

The below progress and process details a few stages followed while working toward the final product. Many stages were excluded in this report as there results were not satisfactory or worth noting.

7.6.1 Initial stage

The initial experimentation was conducted using a function generator, allowing for maximum adjustment while determining the working frequencies of the coil pair with a 1mm airgap. The initial coil design was a large diameter type (250mm diameter), wound from 1mm, core winding shielded copper wire. This was glued onto a 1mm thick Perspex sheet, allowing for an accurate air gap. Figure 55 illustrates the initial design showing the 1 to 1 turns ratio wound at a diameter of 250mm with an airgap of 1mm.

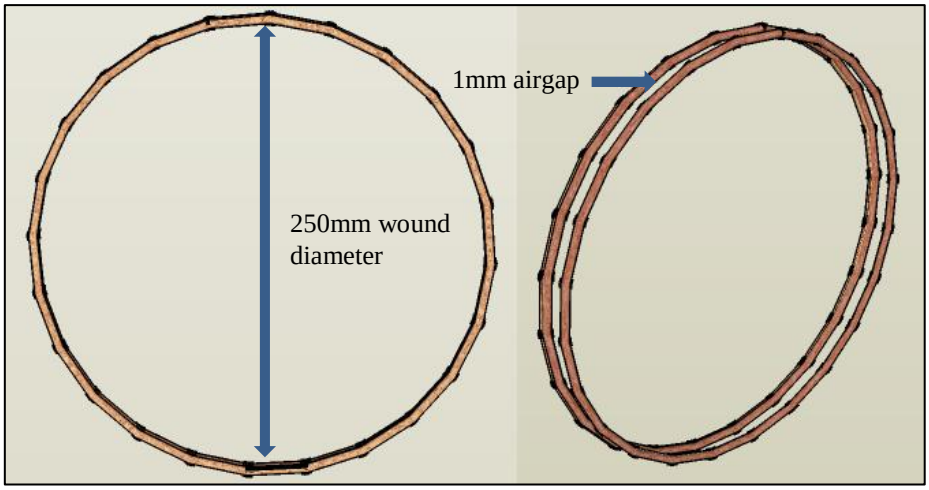

Figure 55: Illustration detailing the first stage of the design using the 250mm diameter 1mm thick wire, glued onto the perspex sheet maintaining the 1mm airgap

The initial electronic design technique for the primary and secondary circuits is now described.

7.6.2 Primary feed

The primary feed electronics remained similar throughout the testing phase, except for minor loading changes on the input, changing the amplitude on the primary coil. The below circuit diagram, in illustration 56 shows the initial circuitry used.

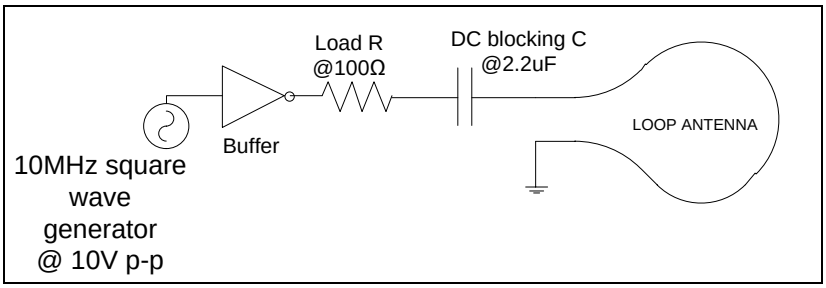

Figure 56: Typical initial primary feed circuitry

7.6.3 Secondary receiving

The Secondary or receiving electronics were altered a few times to allow for an adequate changing voltage gain, between 0V and 5V. The variations used during the experimental phase will be described further. The below circuit diagram, shown in illustration 57 describes the first test-phase circuitry used on the secondary receiving coil.

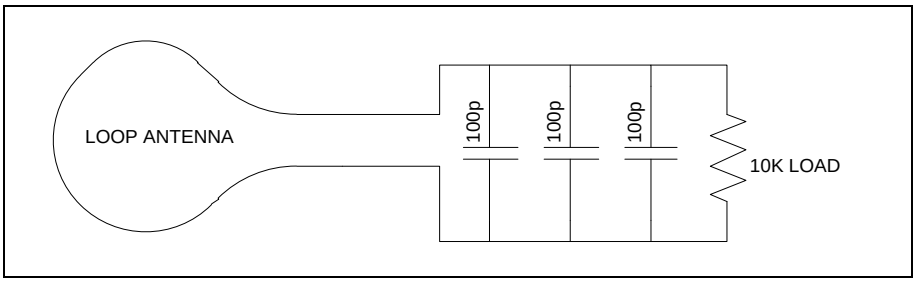

Figure 57: Typical initial secondary circuitry

With the Primary and Secondary in place, a manual frequency sweep was performed. The graph below describes the initial stage tests and results, detailing the manually selected input frequencies versus the output voltage. A frequency sweep example can be seen in Appendix A, detailing the input and output readings of the initial test prototype on an oscilloscope. The function generator was maintained at a constant 10V peak to peak wave. The initial tests were done using many reference points allowing for a higher resolution, this was reduced as the testing progressed, as the high resolution was unnecessary.

The below frequency versus output voltage graph used 41 reference points allowing for the high resolution. The associated values are tabled in Appendix B.

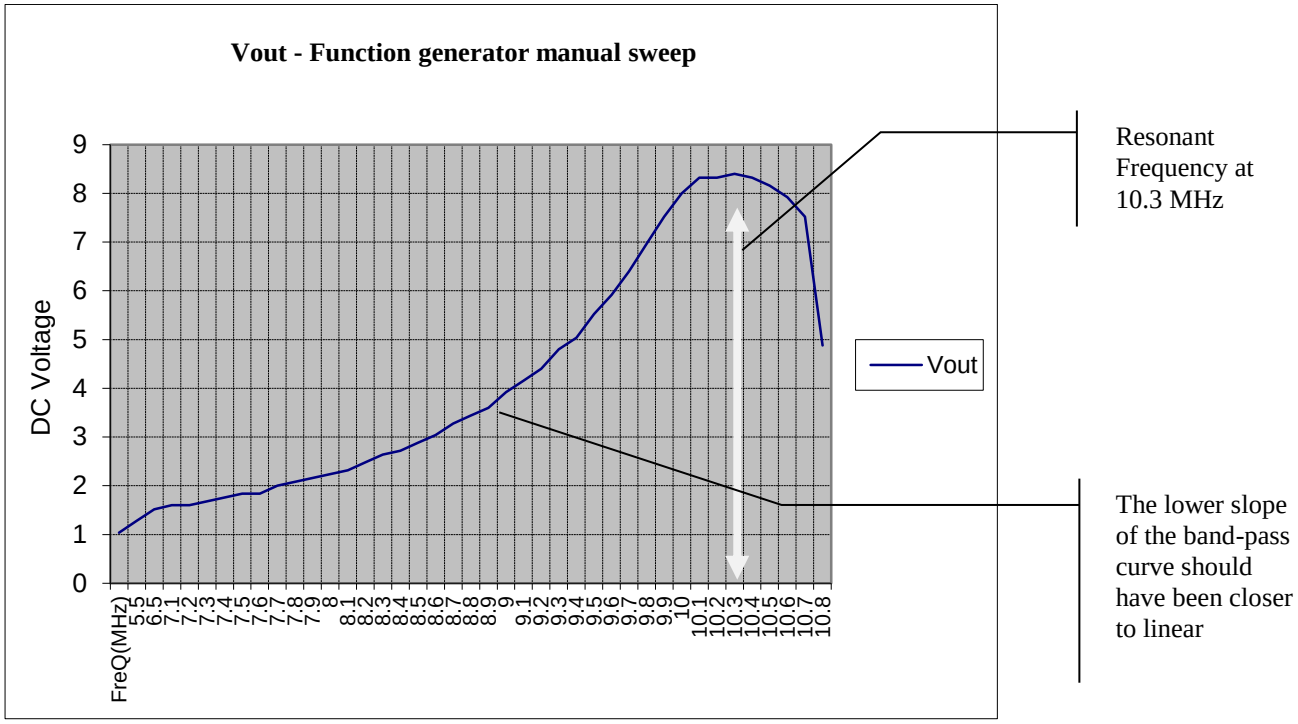

Figure 58: Initial manual frequency sweep test results

7.7 Conclusions to the initial test

The initial testing was conducted using an input voltage of 10V peak-to-peak, set on the function generator, which proved to be unpractical as the requirement was a maximum voltage of 5V. 5V also proved to be more compliant for low voltage electronics. The first tests revealed that the lower slope of the band-pass curve was not sufficiently linear, as visually seen in Figure 58 above. The goal of the experiments was to achieve the closest to linear curve on the lower slope of the curve,

allowing for an even force to electrical output swing around the reference voltage of 2.5V, transmitted over the wireless system from the moving wheel to frame.
Experiment goals after the initial tests:

- Design electronics to generate a useable clean 5V peak-to-peak wave with sufficient frequency to drive the primary coil on the moving wheel.
- Alter the coil specifications allowing for a better suited mechanical design, for mounting on the wheelchair wheel and frame.
- Ensure the coil with the mechanical redesign performs electronically, as desired.
- Redesign the secondary receiving electronics allowing for the designed results. A useable fluctuating voltage referenced at 2.5V changing between 0V and 5V also with a linear lower band pass curve, allowing for a linear force to voltage output transmitted wirelessly.

7.8 Wireless signal transfer design summary

- Electronic design for a 5V square wave generator

  The design called for a frequency generated by a referenced fluctuating voltage. A simple Voltage Controlled Oscillator was utilised. The correctly chosen VCO had the characteristics needed for the high frequency generation, if the parameters were setup correctly.
- Mechanical signal coil redesign

  The large sized signal transfer coils proved to be electronically sound but impractical when trying to achieve the correct 1mm air gap as described earlier. Also the power generation cast coils were already manufactured to the given size, so the decision was taken to couple the two coils together, allowing for a practical mechanical fix. Initially the reduced sized coil was wound out of similar 1mm diameter laminated transformer wire at a ratio of 1:1. Figure 59 below indicates how the initial attempt was setup.

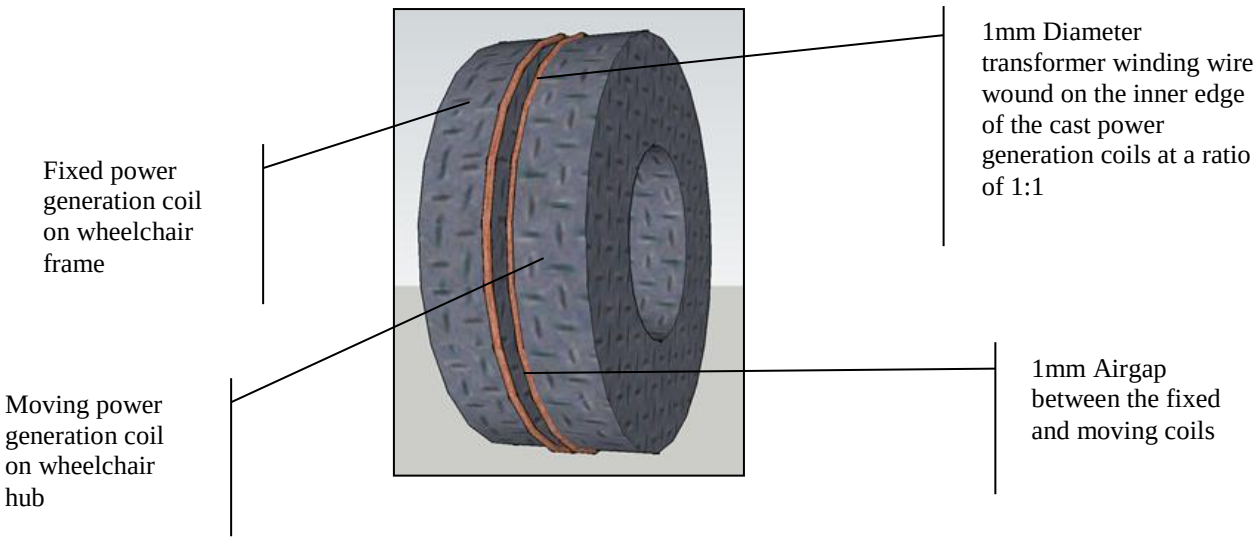

Figure 59: Mechanical redesigned power and signal transfer coil pair with a signal coil turns ratio of 1:1

A similar experiment was performed on the singly wound wire and coil setup, with the following criteria.

- A manual frequency sweep was performed with all component values remaining the same as the initial experiment with the large form coil, with a 1mm air gap and configuration as indicated above.

- Before recording each reference point the output voltage was monitored through the frequency sweep, ensuring that a sufficiently high output voltage was achieved.

The singly wound 1mm wire, as described above did not allow for sufficient voltage generation at the secondary. A minimum of 5V on the secondary was required allowing for a full 0V – 5V swing.

The decision was taken to experiment with the turns ratios of the primary and secondary signal transfer 1mm diameter transformer wire. A 1:2 turns ratio was adopted and the experiment was repeated. Theoretically the 1:2 turns ratio should double the voltage on the receiving side. The 1:2 turns ratio can be seen in the sketch below.

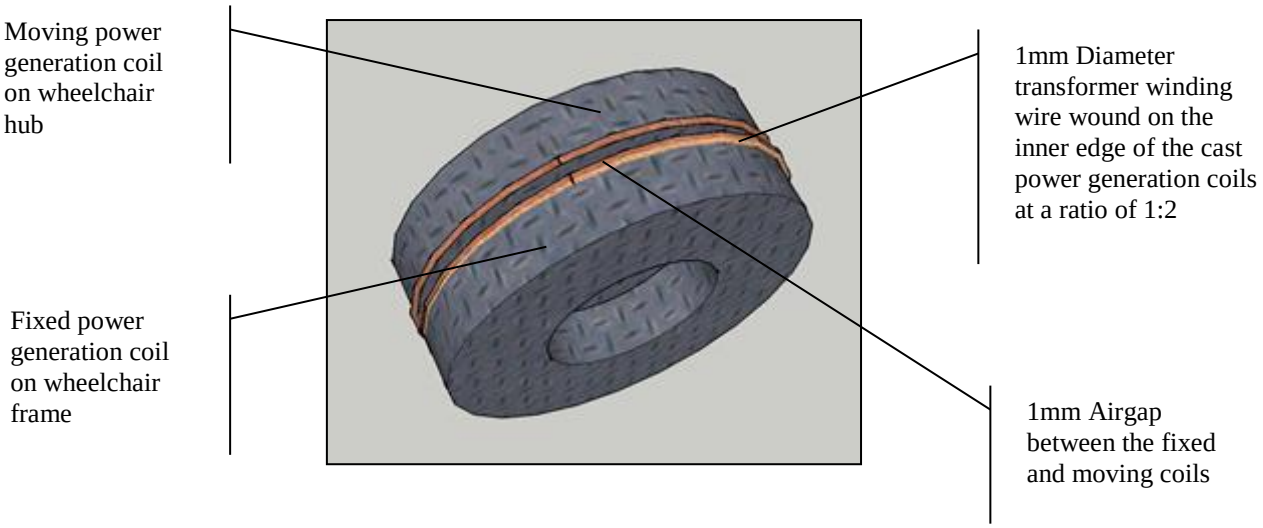

Figure 60: Mechanical redesigned power and signal trasfer coil pair with a signal coil turns ratio of 1:2

The previous experiments were repeated but revealed that the desired output voltage was not achieved again. The upper threshold output voltage of 5V on the secondary was not achieved in any frequency region of the manual frequency sweep, around the resonance of the combined 1:2 turns ratio coils.

7.9 Final wireless signal transfer electronic design considerations

The decision was taken to build a basic voltage doubler circuit into the secondary rectification electronics allowing for an even greater output voltage. The full-wave voltage doubler with rectification electronics used can be seen in figure 61 below.

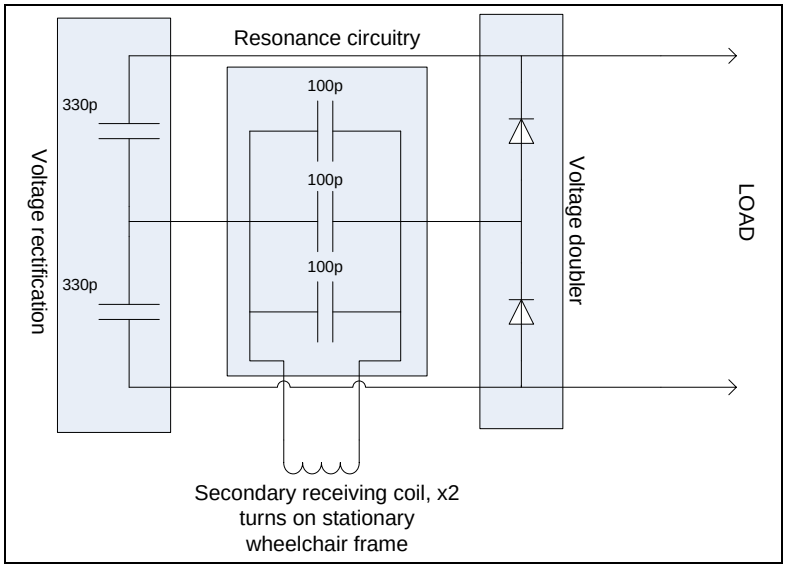

Figure 61: Typical secondary rectification and voltage doubler circuitry

With the voltage doubler and increased turns ratio combination on the secondary the desired generated output voltage was finally achieved after the sequenced experimentation used earlier was repeated. The below, frequency versus output voltage graph and table in Appendix B indicate that the redesigns pushed the output voltage higher than the desired 5V. The goal was to achieve an output voltage that closely resembled the input voltage of the VCO. The input and output voltages should track linearly to ensure correct operations. The output voltage should track the input voltage ensuring the proportional force applied by the user matched the motorised assistance by the hub motors. Slight electronic component variations were considered to fine tune the design to ensure the desired output was achieved. The below output voltage graphs and descriptions detail the fine tuning. Figure 62 below illustrates the output voltage after the voltage doubling electronics were added.

With the newly designed voltage doubler circuitry and coil turns ratio of 1:2 an output voltage of 6.72V was achieved, which was too high

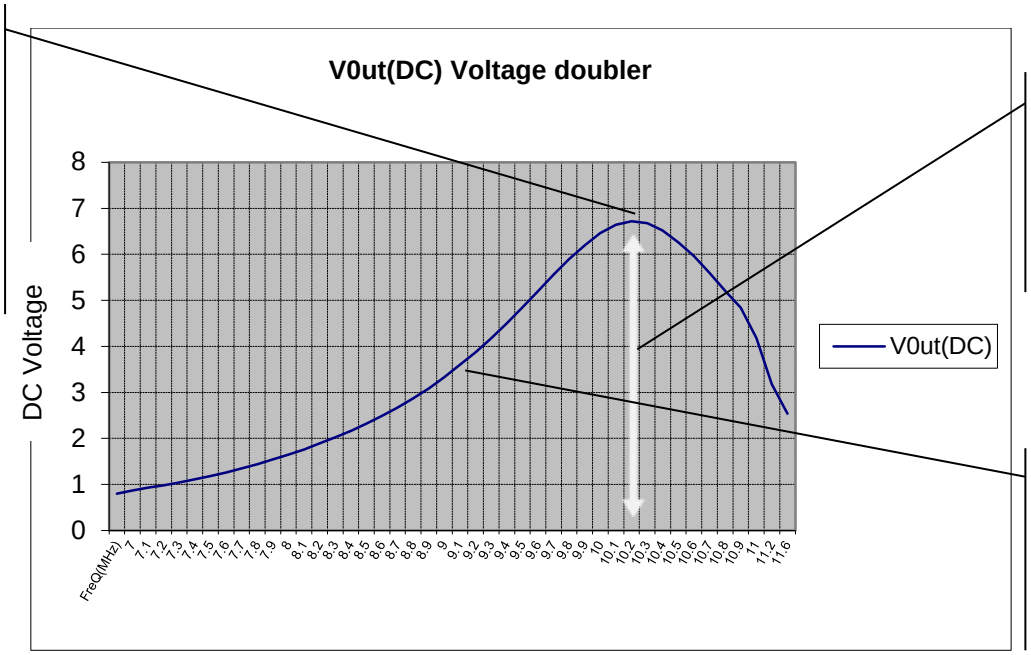

Figure 62: Graph detailing the results found with the signal transfer coils wound smaller at a turns ratio of 1:2 with the voltage doubler on the secondary

The higher than expected output voltage generated at the secondary, after the multiplier circuitry and at resonance of 10.3 MHz needed to be around 5V. The decision was taken not to alter the mechanics of the coils or resonance characteristics as the performance was satisfactory. The final output voltage was lowered by installing three series diodes on the output, with a combined volt drop of around 1.7V. This simple addition allowed for the ideal output voltage swing between 0V and 5V while biased under no load at the 2.5V reference. The final goal was to ensure the lower slope of the band-pass curve was as linear as possible.

Experiments were done on altering the input and output load resistance. The below graph in figure 63 details the input frequency versus the output voltage relationship with a configuration of a 220Ω series resistor on the input of the primary coil and a 6.8kΩ resistor acting as the load on the receiving electronics. The tables can be seen in Appendix B. As described earlier far fewer reference points were used, as the resolution proved to be satisfactory.

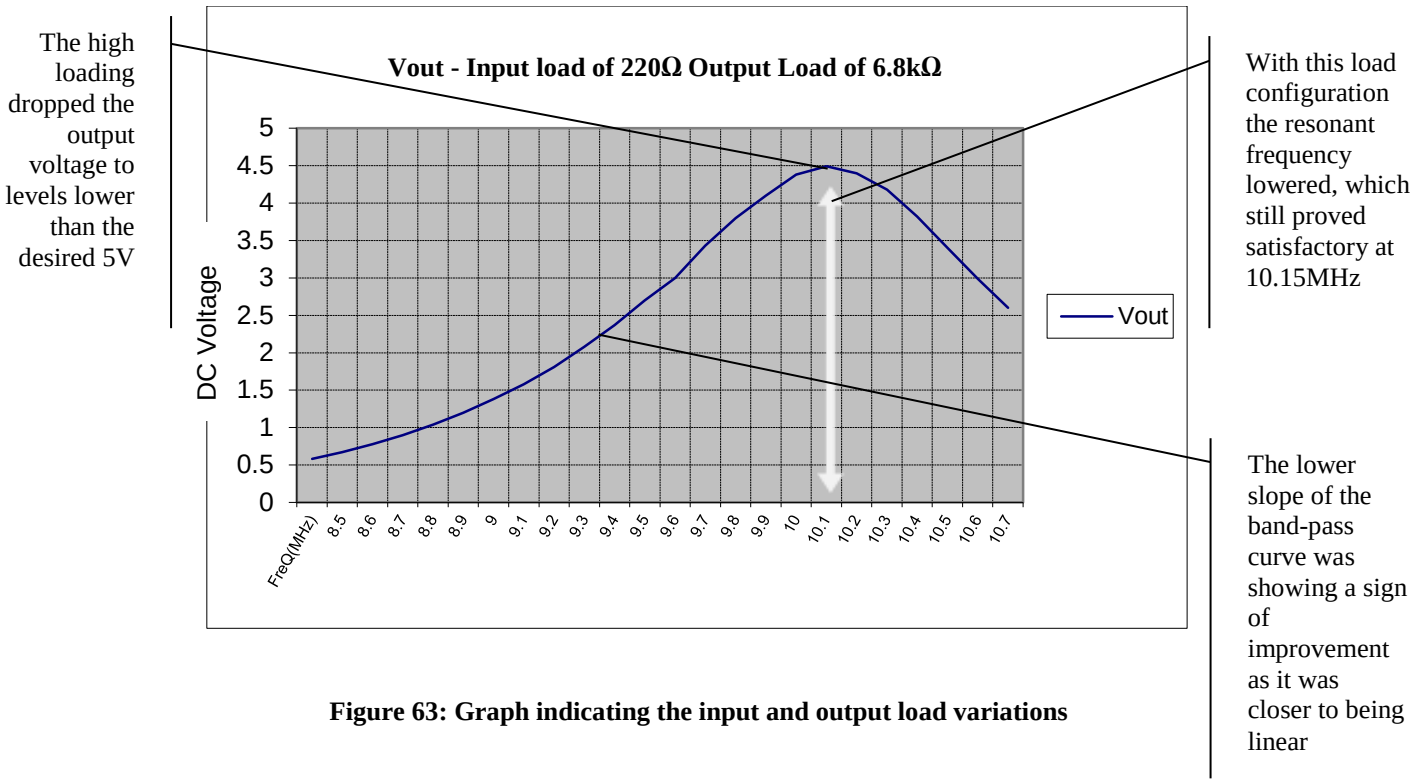

Figure 63: Graph indicating the input and output load variations

The lower slope of the band-pass curve proved to be closer to linear with the input and output loads set at 220Ω and 6.8kΩ respectively. The loading worked negatively on the desired output voltage of 5V, with the maximum output hovering around 4.5V. The input and output load resistors were adjusted and via experimentation the final values were ascertained.

The final prototype circuit input resistance was set at 330Ω while the output resistance was tweaked to a final value of 100kΩ. Any value smaller than the 100kΩ on the output drew higher current values and lowered the output voltage below the 5V thresh hold. The final output table 2 and graph, illustrated in figure 64 are shown below for the prototype on both the left and right wheels are shown below. The graph shows the VCO input voltage VS the output voltage of the secondary. All tests were done while the wheelchair wheels were stationary and in motion.

7.10 Wireless measurement electronics results and conclusions

7.10.1 VCO*in(primary)* versus V*out (secondary)*

Table 2: Final Voltage in VS Voltage out results

Vout (Secondary)	Vin (primary VCO)
1.5	1
1.77	1.5
2.06	2
2.5	2.5
3	3
3.59	3.5
4.2	4

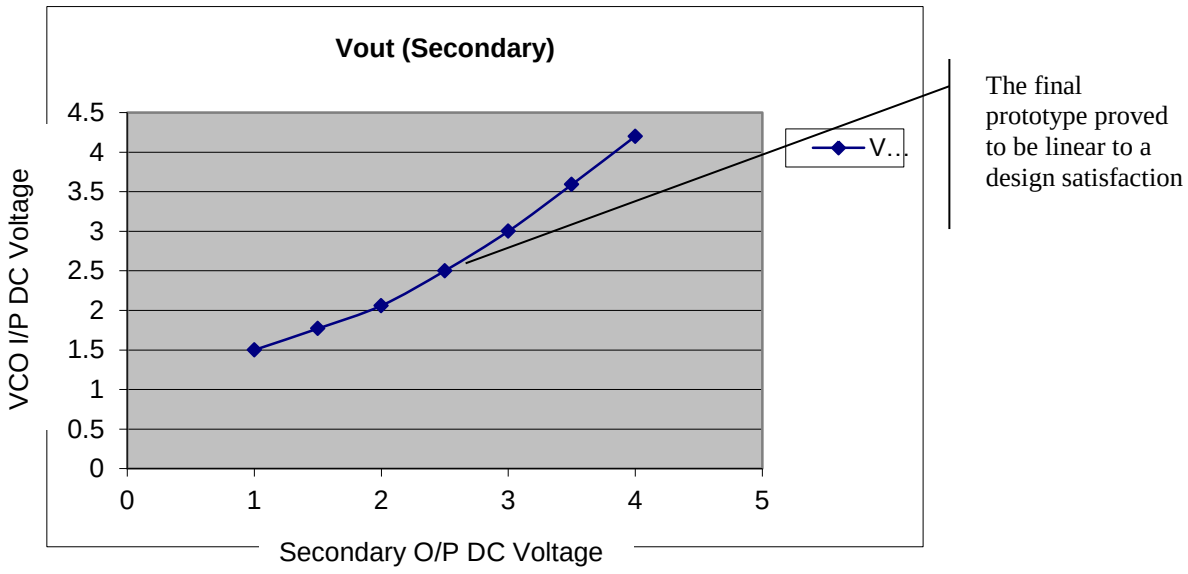

Figure 64: Final prototype graph indicating the final results

The graph above shows the VCO input voltage compared to the wirelessly transferred secondary output voltage, after the slope detection and voltage capping electronics. The Input and output voltages are sufficiently linear as per the original design scope. The final prototype circuit design and flow description can be found in Appendix D.

CHAPTER 8
Overall conclusions and results

8.1 Project overview

The objective of this project was to modify a standard manual wheelchair utilising the units existing large radius wheel design, fixing high torque, three phase hub motors and precision drive electronics onto it while providing the clearance necessary to overcome rough rural Southern African terrains. This also enabled the chair to be used as a manual wheelchair should the battery fail. Research was done on two controller types, namely a static joystick per wheel and a wireless force control system fixed on the independent pushrims on the wheels of the wheelchair. Two types of control techniques were designed to accommodate weak users, debilitated by disease. A consideration for the project required the final product to be cost effective, ensuring the unit be affordable to the poorer communities of Southern Africa. Some final conclusions to the various design phases follow below.

8.2 Wheelchair re-design conclusion

The research highlighted the need for cost effective electric wheelchairs. The majority of existing wheelchair users in Southern Africa utilise manual wheelchairs with many being issued to them by the state. The high number of manual wheelchair users influenced the re-design of a manual wheelchair into an electric unit, using existing electric bicycle three phase hub motors with precision electronics. This also allowed for the modification of a user's existing manual wheelchair to electric at a minimal cost. The design called for a manual wheelchair frame redesign allowing for a fixing technique for the hub motors.

Chapter 3 describes the re-design in detail concluding that the newly modified electric wheelchair could operate within the minimum South African wheelchair ramp specifications with a user weighing 80kg's. The unit was further tested as a pure manual wheelchair with a user of over 100kg, proving that the mechanical design was sufficiently strong for any average weighing user.

8.3 Electric assist option conclusion

The study investigated an electric assist type option on the wheelchair aimed at assisting weak and primarily disease weakened wheelchair users in Southern Africa. A number of different options for measuring the forces applied by wheelchair users on the pushrims of the wheelchair were discussed in the attempt to proportionally assisting the user as they propelled themselves with the wheelchairs existing pushrims.

The force measurement model and prototype were successfully designed and manufactured whereby the user's mechanical force applied on the pushrims was measured on the rotating wheel. The measured force was interpreted by advanced measurement electronics producing a proportional changing output voltage referenced at 2.5V. The measurement electronics designed were used in two different applications in this project, namely the force measurement by the user on the pushrims and the design of a static joystick for manual manoeuvring of the individual wheelchair wheels. Further research was required on powering the measurement electronics wirelessly between the rotating wheel and frame. Research was also required on wirelessly transferring the measured output changing voltage to the wheelchair frame, for interpretation by the hub motor controller. This is discussed further in this conclusion chapter.

8.4 Static joystick design conclusion

Many Southern African wheelchair users suffer from neuro-muscular disorders like Cerebral Palsy and Parkinson's disease restricting their ability to operate a conventional four quadrant joystick. The haphazard hand control motion experienced by such sufferers made the smooth control of a conventional electric wheelchair controlled by a standard joystick impossible. This led to the research and development of a static type two quadrant joystick per wheelchair wheel, controlling the forward and backward motion of the wheels individually. The operation of the unit replicated a track driven vehicle where forward motion required both the left and right wheels to rotate at a similar speed in the same direction. Turning the unit would require less speed on either wheel causing it to turn left or right respectively. This was all controlled by a proportional force applied on either static joystick which in turn replied with a proportional referenced output voltage.

The final joystick prototype consisted of the similar measurement electronics utilised in the force measurement electronics on the wheelchairs pushrims, as described earlier. The output voltage of the joystick was designed to be similar to the output voltage of the measurement electronics, ensuring that similar signal interpretation electronics were utilised on the hub motor controllers for both the force measurement and joystick control techniques. The output was referenced at 2.5V (no user input) and between 2.5V and 5V for a forward input, with a reference of between 2.5V and 0V for a proportional reverse applied force by the user. The full joystick design and final prototype is shown in chapter 5.

8.5 Wireless power generation conclusion

The study discussed a method of user input force measurement on the rotating wheelchair pushrims for the electric assist option. This was successfully achieved by adopting sensitive measurement electronic techniques as detailed earlier. An outstanding issue was powering the electronics technically operating across an airgap on the rotating wheels. Various methods were discussed in Chapter 6 highlighting the transformer type flux coupled model as the preferred power generation method. This was due to the reasonably high power requirement of the measurement electronics.

The final prototype utilised a carefully designed and manufactured primary and secondary coil configuration fixed on the stationary wheelchair frame and moving hub motor and wheel assembly. The coils rotated side-by-side while a 1mm airgap was maintained. The initial experiments yielded insufficient transformer efficiencies resulting in lower than expected power generation on the secondary coil and rectification electronics. This was solved by modifying existing transformer metal laminations and mounting them onto the primary and secondary coils. These were cast in a polymer mixture creating two similar circular robust structures. The laminations provided a direct path for the flux from the primary coil to the secondary via the 1mm airgap. With the addition of the laminations and carefully configuring the driving and receiving electronic circuits the wireless power generation objective was met. The required 35mA at 6-7V was generated at the secondary which was

necessary to power the measurement electronics mounted on the wheelchairs rotating wheel. The detailed design is discussed in Chapter 6.

8.6 Wireless measurement electronic signal transfer conclusion

The prototype force measurement electronics were successfully designed and manufactured allowing for the proportional, user applied force measurement and changing voltage output. This changing output DC voltage referenced at 2.5V was required to reference the hub motor controllers allowing for the electric kinetic assist option detailed earlier. The similar issue was introduced as previously discussed in the power generation chapter of wireless transferred power and now signal. The real time analogue single needed to be wirelessly transferred between the rotating wheelchair wheel and the static wheelchair frame. A number of techniques were discussed in this dissertation from slip rings to the RF method. The RF method was considered but ruled out due to the high resolution requirements resulting in high costs of the RF electronics, as discussed in Chapter 7.

The final solution incorporated a similar design technique adopted by the power transfer method, by utilising tuned primary and secondary coil circuits. Various experiments were required to fine tune the design, which resulted in a product that successfully met the project objectives. The output voltage on the secondary tuned signal transfer circuit located on the static wheelchair frame closely matched the output voltage swing of the measurement electronics, concluding that the design was sound.

8.7 Project obstacles and limitations

The electronic design techniques adopted were basic electronic fundamentals but a few obstacles were discovered during the research and development phase. Some examples were as follows:

- Laminations were required in the power coil design. The first power coil design was done using iron filings mixed in with the polymer. This design tactic did not allow for sufficient electromagnetic energy to be transferred

from primary to secondary, therefore the inclusion of laminations in both coils solved this problem by allowing a direct path for the eddy currents. The air gap needed to be kept at a minimal to avoid any interference.

- Careful PCB layouts and designs allowed for minimal noise so assisting in stable reference voltages and VCO outputs.
- VCO setup was crucial in achieving the correct resonant frequency and frequency range so to allow for accurate slope detection on the secondary.
- The resonant frequency changed drastically once the coils were mounted onto the frame. The system needed to be readjusted in the final prototype.
- Further research and development with the design could refine it drastically. The final wirelessly transferred force to voltage signal referenced at 2.5V, fluctuating between 1V, negative force on the pushrim and 4V, positive force on the pushrim would be utilised in the Hub Motor controller, which was out of scope.

Considering the limitations all the project goals and objectives were met. The final prototype circuit diagrams with project phase descriptions follows in Appendix C, D and E.

BIBLIOGRAPHY

1. Bergasa, LM. Mazo, MA. Gardel, R. Barea, L. Boquete, 2000. *Commands generation by face movements applied to the guidance of a wheelchair for handicapped people,* 15th International Conference Volume 4, pp 660 - 663

2. Brown, K.E. Inigo, R.M. Johnson, B.W. 1990. *Design, implementation, and testing of an adaptable optimal controller for an electric wheelchair,* Industry Applications, IEEE Transactions, pp 1144 - 1157

3. Chikkum, DR. 2002. *Performance of disk brushless DC motor applied as gearless drive for wheelchair, B-Tech J. N. T. U 2002*

4. Choi, C-H. Seo, Y-C. Kim, S. 2004. *Brushless DC Motor Controller for Tele-operational using embedded real-time LINUX,* 30th Annual Conference of the IEEE Vol 3, pp 2952 – 2956

5. Chu, J-U. Moon, I-H. Choi, G-W. Ryu, J-C. Mun, M-S. 2004. *Design of BLDC Motor Controller for Electric Power Wheelchair,* Korea Orthopedics & Rehabilitation Engineering Centre (KOREC).

6. dos Santos, JLA. Dos Anjos, EG. 2011. *Department of Informatics Engineering, University of Coimbra, 3030-290*

7. Drewniak, J.L. *Coupling Through the Magnetic Field --- Faraday's Law,* EMC Laboratory, University of Missouri-Rolla, retrieved 3rd August 2011 from http://www.emcs.org/edu/ExperII/MagFieldCoupling.pdf.

8. Filho, ACL. Belo, FA. dos Santos, JLA. dos Anjos, EG. 2010. *Experimental and theoretical study of a telemetric dynamic torque meter,* J. Braz. Soc. Mech. Sci. & Eng. vol.32 no.3

9. Fezari, M. Bousbia-Salah, M. Bedda, M. 2005. *Computational Intelligence Methods and Applications,* ICSC Congress, pp 5.

10. Gieschke, P. Richter, J. Joos, J. Ruther, P. Paul, O. 2008. *Four-degree-of-freedom solid state MEMS joystick,* IEEE 21st International Conference, Micro Electro Mechanical Systems, pp 86-89.

11. Kaminska, B. Mahanfar, A. Mazlouman, S.J. 2009. *Mid-range wireless energy transfer using inductive resonance for wireless sensors,* IEEE International Conference on Computer Design (ICCD), pp 517-522.

12. Karalis, A. Joannopoulos, J.D. Slojačić M. 2008. *Efficient wireless non-radiative mid-range energy transfer.* Annals of Physics, vol 323, no. 1, pp 34-48

13. Kevin, B. Stanton, PR. Sherman, ML. Rohwedder, CP. Fleskes, DR. Gray, DT. Minh, CE. Dieudonne, Ishaque, MM. and Perkowski, MA. 1990. *PSUBOT – A voice controlled Wheelchair for the handicapped*, Circuit and Systems, pp 669-672.

14. Kurozumi, R. Yamamoto, T. 2005. *Intelligent Robots and Systems,* IEEE/RSJ International Conference, pp 1108-1113

15. Li, H. Yan, G. Gao P. 2010. *A method for improving the wireless power transmission efficiency of an endoscopic capsule based on electromagnetic localization and synthesis of magnetic field vector,* Proceedings of the Institution of Mechanical Engineers, Part C: Journal of Mechanical Engineering science 224:1463.

16. Leung, C.C. Chan, T.P. Lit, K.C. Tam, K.W. Chow, L.Y. 2010. *Wireless Power Transmission and Charging Pad,* The Hong Kong Institute of Vocational Education (Tsing Yi).

17. Lu, H. Kim, H. Lee, JM. Li X. 2006. *Joint Joystick Based on Linear Compensation* 6th International Conference, Intelligent System Design and Applications, 6th International Conference Vol 2, pp 66-71

18. Matthews, MA. 2006. *The design and development of an electric wheelchair,* B-Tech, CPUT.

19. Maxim Integrated Products, 2005. *7.6A, 12ns, SOT23/TDFN, MOSFET Driver,* Product data sheet Rev 4; 7/05.

20. Mercotac, Inc. *How does a Slip Ring work?* Retrieved 2nd August 2011 from http://www.mercotac.com/html/slip-ring.html

21. Myers, BA. Wobbrock, JO. 2005. *Human-Computer Interaction,* 11th International Conference, pp 22-27

22. Naudé, V. 2006. *Quotation of electric wheelchairs,* October 2, 2006 Medop cc

23. Propentia (PTY) Ltd 1999. *User Report Wheelchair Survey,* Project for the SA National Department of Health February, pp 18-19, pp34.

24. Picture of a manual wheelchair [Online] Available: http://www.glad.netproductimagesM4VBIG.jpg [Last Accessed: 10 October 2006], August 2006.

25. The Robot Market Place. *Powersonic battery prices* [Online]. Available from: http://www.robotcombat.com/products/0B-PS-605.html [Accessed: 2nd August 2011].

26. RSA National Government, 2006. *National Building Regulations, Part S: Facilities For Disabled Persons.*

27. Williams, D.B. Carter, C.B. 2009. *Transmission Electron Microscopy: A Textbook for Materials Science.* New York: Springer Science + Business Media, LLC.

28. James, R. Carstens, P.E. 1993. *Electrical Sensors and Transducers*, New Jersey: REGENTS/PRENTICE HALL.

29. ANALOG DEVICES, 2005. *AD620, Low Cost, Low Power Instrumentation Amplifier*, Product data sheet Rev E.